STAGE DISCHARGE ESTIMATION USING A 1D RIVER HYDRAULIC MODEL AND SPATIALLY-VARIABLE ROUGHNESS

by

Timothy John Blair

B.Ap.Sc., University of British Columbia, 2006

A THESIS SUBMITTED IN PARTIAL FULFILLMENT OF THE REQUIREMENTS FOR THE DEGREE OF

MASTER OF APPLIED SCIENCE

in

The Faculty of Graduate Studies

(Forestry)

THE UNIVERSITY OF BRITISH COLUMBIA
(Vancouver)

December 2009

ABSTRACT

Stage-discharge relations (rating curves) are integral to stream gauging, yet the existing empirical calibration methods are expensive, particularly in remote areas, and are limited to low flows. Numerical modelling can provide stage-discharge relations from a single site survey, reducing the overall cost, and can be fit to changing surface conditions. This study explores a one-dimensional model to calculate theoretical stage-discharge relations for four field sites in British Columbia that range in bed stability, bed structure, hydrology and sediment supply. However, due to the non-linear relation between flow and roughness we do not assume the conventional reach-averaged roughness and instead employ a spatially-distributed roughness model. Furthermore, based on local grain size distribution and refined field survey technique, new formulae for wetted perimeter, flow area, and flow depth were developed that eliminate commonly held modelling assumptions and reduce topographic error. The results show (1) good agreement with Water Survey of Canada measurements, (2) distributed roughness provided an improvement over spatially-averaged roughness, (3) spatial variability of the geomorphology within the channel reach leads to shifts in the stage-discharge relations and high sediment amplifies those shifts, and (4) the relations must be re-evaluated following events that mobilize the bed. The method can be used to estimate high flows and flows in remote locations and it does not require calibration.

TABLE OF CONTENTS

Abstract ii
Table of Contents iii
List of Tables iv
List of Figures v
Acknowledgements vi
Nomenclature vii
Statement of Collaboration vii
1 Introduction: 1
2 Theory 4
3 Study Sites 7
4 Method 21
4.1 Numerical Model 21
4.2 Field Surveys 26
5 Model Results and Discussion 31
5.1 Alouette River 31
5.2 Cayoosh Creek 33
5.3 Baker Creek 36
5.4 East Creek 38
6 Conclusion 43
7 References 45
Appendices 51
Appendix A: Derivation of Geometric Formulae 51
A.1 Cross-sectional Area of Flow 51
A.2 Flow Depth 53
A.3 Calculating the Wetted Perimeter 54
A.4 References 56
Appendix B: Bed Roughness 57
B.1 Review 57
B.2 Wiberg and Smith (1991) Roughness Model 58
B.3 References 62

LIST OF TABLES

Table 1: Spatially-averaged grain-size statistics. 28

LIST OF FIGURES

Figure 1: Location of field sites 8
Figure 2: Alouette River watershed 9
Figure 3: Alouette River study site and nearby reach 10
Figure 4: Alouette River photo from bridge looking upstream 10
Figure 5: Alouette River modeled reach 11
Figure 6: Cayoosh Creek watershed 12
Figure 7: Cayoosh Creek study site and nearby reach 13
Figure 8: Cayoosh Creek photo looking downstream from bridge 13
Figure 9: Cayoosh Creek modeled reach 14
Figure 10: Baker Creek photo looking upstream from bridge 15
Figure 11: Baker Creek watershed 16
Figure 12: Baker Creek study site and nearby reach 16
Figure 13: Baker Creek modeled reach 17
Figure 14: East Creek photo looking downstream. 19
Figure 15: East Creek modeled reach 19
Figure 16: East Creek watershed 20
Figure 17: Method flow chart 21
Figure 18: Visual depiction of the geometric parameters used in the study 22
Figure 19: Sample of spatially-variable roughness data for the modeled reach of Cayoosh Creek. 28
Figure 20: Comparison between the spatially-averaged and spatially-variable grain-size distributions 29
Figure 21: Gaussian fit of the measured stream roughness. 30
Figure 22: Alouette River model verification using measured data from 32
Figure 23: Cayoosh Creek model verification using measured data from 34
Figure 24: Close-up of riffle at downstream end of the gauge-pool at Cayoosh Creek. .. 35
Figure 25: Baker Creek model verification using measured data 37
Figure 26: East Creek modeled stage-discharge at various pins for multiple years 40
Figure 27: East Creek surveyed bed shape at various pins for multiple years 41
Figure 28: East Creek surveyed bed shape immediately downstream of the modelled locations for Pin #40 and #41 42
Figure A.1: Parabolic representation of a single sediment grain 29 55

ACKNOWLEDGEMENTS

Grateful thanks to Dr. Younes Alila, Dr. Marwan Hassan, and Dr. Rob Millar of the University of British Columbia, for their excellent supervision, ideas, and encouragement throughout my M.A.Sc. program. Special thanks are owed to Jason Kean, for supplying his initial model, Ned Andrews for his encouragement, and Stuart Hamilton and particularly Dave Hutchinson from the Water Survey of Canada for their help, insight and enthusiasm.

I also appreciate help in the field from Rich So, Dr. Phil Marren, Dr. Dan Bewley, Dr. Michael Church and Mirella Mazur. In addition I would like to thank Josh Caulkins and his assistants for helping to gather the survey data at East Creek.

Finally, I would like to express my sincere appreciation for the financial support provided by Dr. Younes Alila, the faculty of Forestry, the University and particularly the National Science and Engineering Research Council Discovery Grants (YA and MAH) and CGS Scholarship (TJB).

NOMENCLATURE

$\overline{A}_D$	protruding cross-sectional area perpendicular to the approach velocity of an average single grain
$\overline{A}_{grains}$	protruding cross-sectional area of the bed roughness perpendicular to the approach velocity
A_{flow}	wetted cross-sectional area of flow
A_{topo}	cross-sectional area of flow from topographic survey
B	wetted channel width
B_i	wetted width of subsection (i)
C	Chezy friction coefficient
c_m	probability of the m^{th} gain size class
d_{50}	median pebble diameter (surface)
d_{84}	pebble diameter - 84^{th} percentile (surface)
$D_{b\text{-}axis}$	intermediate axes of the grains
D_x	same as $D_{b\text{-}axis}$
D_z	vertical axes of the grains
$D_{z,m}$	intermediate axes of the 'm' grain size class
f	Darcy Weibach friction factor
Fr	Froude number
g	acceleration of gravity
h_{topo}	stream depth from water surface to the survey line
h_{flow}	wetted stream depth accounting for boulders above the survey line
i	identifier for the discrete subsections within a cross-section
I	total number of subsections in each cross-section
LWD	Large Woody Debris
m	grain size class
M	total number of grain size classes
n	manning's roughness
P_{flow}	wetted perimeter including shape of roughness elements
P_i	P_{flow} for subsection (i)
P_{topo}	wetted perimeter along the survey line
Q	discharge
R_{flow}	Hydraulic Radius based on A_{flow} and P_{flow}
R_{topo}	Hydraulic Radius based on A_{topo} and P_{topo}
s_1	shape factor for grains
S_f	friction slope
S_o	bed slope
$WS_{critical}$	Critical water surface elevation
u	flow velocity
u_*	shear velocity
$\overline{u}$	depth averaged flow velocity
u_{ref}	drag reference velocity
WSC	Water Survey of Canada
x	streamwise direction
y	transverse direction
z	vertical direction
z_o	roughness length of the log-law
β	momentum correction factor
θ_i	proportion of the subsection width (B_i) taken up by the width of one average grain
κ	Von Karman coefficient
λ	vegetation density
σ_d	dimensionless vegetation deceleration
σ_{ϕ_x}	standard deviation of the pebble
ϕ	phi notation for grain size ($\phi = -\ln_2(D_x)$)

STATEMENT OF COLLABORATION

This thesis will be revised into a manuscript co-authored with Dr. Younes Alila and Dr. Marwan Hassan at the University of British Columbia. As the first author, I was in charge of all aspects of the project including formulating literature review, research design, model construction, and results analysis. I collected all data pertaining to the Alouette, Cayoosh and Baker field sites. The topographic and roughness data from the East Creek field site were collected by Andre Zimmermann in 2003, Joshua Caulkins in 2004 with Caulkins, Zimmerman and Toby Perkins in 2005, Caulkins and Tony Lagemaat in 2006, and Lagemaat in 2007 and 2008. East Creek also involved several field assistants and was supervised by Dr. Marwan Hassan.

1 INTRODUCTION:

The primary method to determine stream flow is to measure the stage and convert it to discharge using a pre-determined stage-discharge relation, typically an empirical relation, derived from expensive manual measurements. Each measurement is only a snapshot in time and the resulting relation is, at best, time averaged as it is averages the manual measurements over the months or years the measurements were recorded. Unfortunately, due to cost and safety limitations many curves are based on a handful of low flow measurements, particularly in remote areas, exacerbating the errors in the estimation of high flow discharges. The stage-discharge relation is the result of a balance between gravity and frictional shear stress forces. In streams the geometry varies and the two forces are never in perfect balance, with local accelerations and decelerations based on local changes in the slope and roughness that cause the stage to have a non-linear relation with discharge.

Several methods have been developed to derive, adjust, and determine the confidence in empirical stage-discharge relations (Gawne and Simonovic, 1994; DeGagne et al., 1996; Herschey, 1999; Moyeed and Clarke, 2005; Pappenberger et al., 2006; Shrestha, 2007; Schmidt and Yen, 2008; Baldassarre and Montanari, 2009; and Souhar and Faure, 2009). Most methods assume stable channels and use empirical models including power law (Chen and Chiu, 2004; and Pappenberger et al., 2006), Manning's equation (DeGagne, 1996; and Leonard et al, 2000), statistical models (Gawne and Simonovic, 1994; and Sivapragasam and Muttil, 2005), pseudo-likelihood regression (Lee et al, 2009) and artificial neural networks (Bhattacharya and Solomatine, 2005). These models require calibration to either specific discharge measurements or to an existing stage-discharge relation, and are therefore not independent of the original stage-discharge relation they are meant to support. As a result, discharge extrapolation using statistical (e.g., Dose et al., 2002; Sivapragasam and Muttil, 2005; Lohani et al., 2006; and Herschy, 2008) and empirical (Leonard et al, 2000; and Pappenberger et al., 2005) methods have remained unreliable.

Gauging sites are ideally established upstream of a critical flow device, or a narrowing of the stream that induces critical flow control (Herschy, 2008). The stage-discharge relation must be re-established following changes in the control, or changes in the channel bed composition (texture and structure) and morphology. These changes can be on a local scale (DeGagne, 1996) or on a reach scale (Juracek and Fitzpatrick, 2009), and they typically occur during major events. To overcome the shifting of relations due to channel instability the current empirical approach requires numerous manual measurements (Braca, 2008; and Herschy, 2008). Alternatively DeGagne et al. (1994), Kean and Smith (2005) and Juracek and Fitzpatrick (2009) suggested relating the stage relation to the bed surface composition. However, modelling sediment transport and channel morphology remains a challenging topic (Cao and Carling, 2002) and most investigations are qualitative and empirical (Smart, 1999; Herschy, 2008; McMillan et al., 2009).

Numerical models are under-utilized and could provide more insight into the impact of channel instability on stage-discharge relations. Kean and Smith (2005) developed a promising numerical method that overcame many of the above-mentioned problems. They proposed a force balance model to calculate the vertical velocity field and combined that with the one-dimensional St. Venant momentum balance equations to calculate the stage-discharge relation. In their approach, Kean and Smith (2005) included a vegetation drag model, based on stem density, with a simple eddy viscosity model to derive a new 'log-law' formulation for the vertical velocity profile. The velocity profile enabled calculation of the Boussinesq momentum coefficient and the friction slope for the momentum balance. They verified the model for high flows using two geomorphically stable study reaches in Kansas with relatively uniform bed surface and fine to gravel sized bed material (?? Kean and Smith, 2005 p.3,8); Kean and Smith suggested further testing before it could be widely used.

The main objectives of this paper are to critically test and further develop the Kean and Smith model, under a range of flow and sediment supply regimes in British Columbia, Canada. To achieve our goals, four stream sites covering a range of channel morphologies, sediment supply regimes, and hydrology from snow dominated to rain dominated watersheds were studied. The examined streams represent stable (two sites) and unstable (two sites) reaches with two different roughness parameterizations. Due to the non-uniform bed surface at our sites, we did not assume spatially-averaged grain-size distributions, and instead we applied detailed bed surface texture and topography (elevation). To investigate the change in stage-discharge relation for an unstable bed the model results were compared to manual discharge measurements before and after a major flood; the model was also applied to a site where multiple years of survey data were available.

2 THEORY

The basis of the numerical model is the one-dimensional St. Venant equations for the momentum balance coupled with two different models for the vertical velocity profile to incorporate roughness (Kean and Smith, 2005). Lateral bank stresses were neglected due to large width-to-depth ratio for all sites (see below for study site description) and all of the model parameters were measured in the field.

The St. Venant equations assume hydrostatic conditions with gradually varying, steady state flow and neglect cross-circulation. The St. Venant equations (1)-(3) are derived in Chow (1959).

$$gS_o A_{flow} - gA_{flow} S_f = \frac{\delta\left(\beta Q^2 / A_{flow}\right)}{\delta x} \tag{1}$$

$$S_f = \frac{Q^2}{gR_{flow}\left(CA_{flow}\right)^2} \tag{2}$$

$$\beta = \frac{A_{flow}\iint u^2 \,\mathrm{dxdy}}{\left(\iint u \,\mathrm{dxdy}\right)^2} \tag{3}$$

The discharge (Q) is a function of the water slope (S_o), the cross-section area of flow (A_{flow}), gravity (g), hydraulic radius (R_{flow}), Chezy coefficient (C), velocity (u), friction slope (S_f), and the Bousinesq coefficient (β). In this study, the roughness model is incorporated into the calculation of C and β.

For gravel and cobble dominated beds the Chezy and Bousinesq coefficients were calculated using a logarithmic velocity profile (equation (4)) (Kean and Smith, 2005), and the roughness length (z_o) was calculated as $z_o = 0.1\ D_{84}$, where D_{84} is the diameter of sediment at the 84^{th} percentile of the grain size distribution (Whiting and Dietrich, 1990), using an assumed log-normal distribution (Wiberg and Smith, 1991, and Nikora et al., 1998). This was coupled with a simple vegetation drag model (Kean and Smith, 1991).

$$\frac{\bar{u}}{u_*} = \frac{\text{depth averaged velocity}}{\text{shear velocity}} = \frac{1}{\kappa}\left[\ln\left(\frac{h_{flow}}{z_o}\right) - 0.74\right] \tag{4}$$

$$C = \frac{1}{A_{flow}\sqrt{R_{flow}}}\int \frac{\bar{u}}{u_*}\sqrt{\frac{h_{flow}}{1+\sigma_d}}dy \tag{5}$$

$$\sigma_d = \frac{1.2}{2}\lambda\left(\frac{\bar{u}}{u_*}\right)^2 h_{flow} \tag{6}$$

κ is von Karman’s constant, the depth of flow (h_{flow}) is calculated below, and the dimensionless vegetation deceleration (σ_d) is based on the vegetation density λ (Kean and Smith, 2005), otherwise known as the frontal area of vegetation per unit volume (Wu et al., 1999), and has units of L^{-1}. Alternative formulations of the vegetation impact on flow have been suggested including foliage drag (Fischenich and Dudley, 2000), fully submerged vegetation\ (Freeman et al., 2000), reduced drag in flexible vegetation (Jarvela 2002), and the flow field within the vegetation (Stephan and Gutknecht, 2002, and Huthoff et al., 2006). However, we decided to use Kean and Smith (2005) vegetation roughness model (presented in equation 6) because of its simplicity in field measurements and it works.

Wiberg and Smith (1991) computed a spatially averaged velocity profile over rough beds, which was also used by Kean (2003) and Carney et al (2006), and was used for boulder dominated beds in this study. The Wiberg and Smith method breaks the total shear stress into turbulent shear stress and shear stress arising from the form drag of grains in the stream bed, and the form drag values are averaged over the grain size distribution. The method uses a simple turbulence closure (Carney et al., 2006), and as the relative roughness decreases the Wiberg and Smith velocity profile approaches logarithmic. Carney et al. (2006) concluded that the Wiberg and Smith velocity profile was “clearly superior to the standard log law” for three coarse-grained streams ($0.1 < D_{84}$/flow depth < 0.3). Assumptions within the Wiberg and Smith model include: 1) there was no blockage of flow by sediment; 2) the grains are not stacked and their bottoms rest on a collective plane; 3) the roughness is well sorted and randomly distributed; 4) the grains are independent such that shadowing effects are neglected; 5) the grains have their short axis aligned to vertical; and 6) roughness element spacing is neglected. The first three assumptions are further discussed through the methods used in this study. The impact of assumptions 4, and 5 are considered in the results and assumption 6 was discussed by Carney et al. (2006). See Appendix B for review of alternate bed roughness formulations and further description of the Wiberg and Smith model.

3 STUDY SITES

Four field sites were selected for our study representing a range of flow regimes and channel morphologies: Cayoosh Creek, Baker Creek, Alouette River, and East Creek (Figure 1). The Cayoosh Creek, Baker Creek and Alouette River field sites are well-established gauging stations run by the Water Survey of Canada (WSC). East Creek has been an ongoing field sediment transport and channel morphology monitoring research site since 2003. The field surveys for the WSC sites were conducted in August 2008 and manual stage discharge measurements were recorded by the WSC from 2007 to 2009. The surveys for East Creek were conducted in each of the six summers (2003 to 2008).

The three WSC field sites cover a wide range of bed composition (texture and structure), flow and sediment supply regimes, channel morphologies, and bed stability conditions. These sites were intentionally selected to contrast the relatively stable Kansas streams studied by Kean and Smith (2005).

There have been recent advances in modelling hysteresis in stage-discharge relations (Lohani et al, 2006, Petersen-Øverleir, 2006, and Braca, 2008), but it has been noticed that the stage-discharge relations developed by the WSC sites don't show a hysteresis between the rising and falling limbs of the flood wave. This is likely due to effective downstream controls combined with the regulated flow at Alouette, and the nival freshet originating from various elevations combined with routing effects at Cayoosh and Baker. Hence the flood wave at all three sites have gentle rising and falling limbs. The control ensures the gauge is not backwatered and the long wavelength is more than an order of magnitude larger than the distance between the controls and the gauges. This is also in contrast to the rapid response and hysteresis noted at field sites of Kean and Smith, which have pluvial flow regimes.

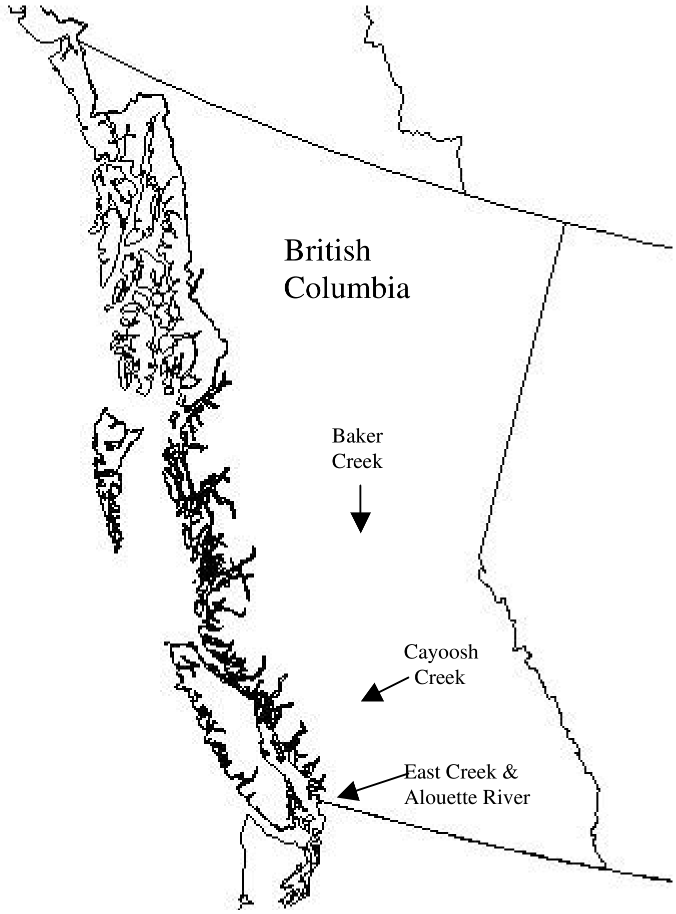

Figure 1: Location of field sites

Alouette River (WSC# 08MH005, 49°14” N, 122°35” W) drains a 235 km^2 watershed, with negligible glacial influence, and a pluvial regime with peak flows occurring from October to March. The study site is located about 12 km downstream of Alouette Lake (Figure 3). Dammed in 1925 there is a diversion of out of the lake for hydroelectricity that bypasses the study site. The maximum recorded flood and mean discharge of the Alouette River are 236 m^3/s and 5 m^3/s, respectively, and the watershed elevations range from 20 m to 2040 m. The primary biogeoclimatic zones of the watershed is Coastal Western Hemlock and the landuse is primarily forest with limited urbanization (< 2.5% of the basin).

Alouette Lake drains 85% of the watershed and captures all sediment upstream of its mouth. Immediately downstream of the lake, the channel is dominated by step-pool morphology with large boulder clusters and limited large woody debris (LWD) for 1 km indicating that the bed is relatively stable with marginal sediment transport rates. At the study site, riffle-pool morphology dominates the channel and the bed is composed of gravel, cobbles and some small boulders. Bars (formed before the dam closure), localized bank erosion, small steep tributaries, and Mud Creek are the main sources of sediment to the study site (Figure 3). There has been no extraction of gravel from the river since the 1990's and since 1999 BC Hydro has created numerous LWD tail-outs for fish and gravel as well as diverting the Mud Creek sediment and replacing it with clean, sorted gravel for fish spawning (BCCF, 1999, 2005, 2006).

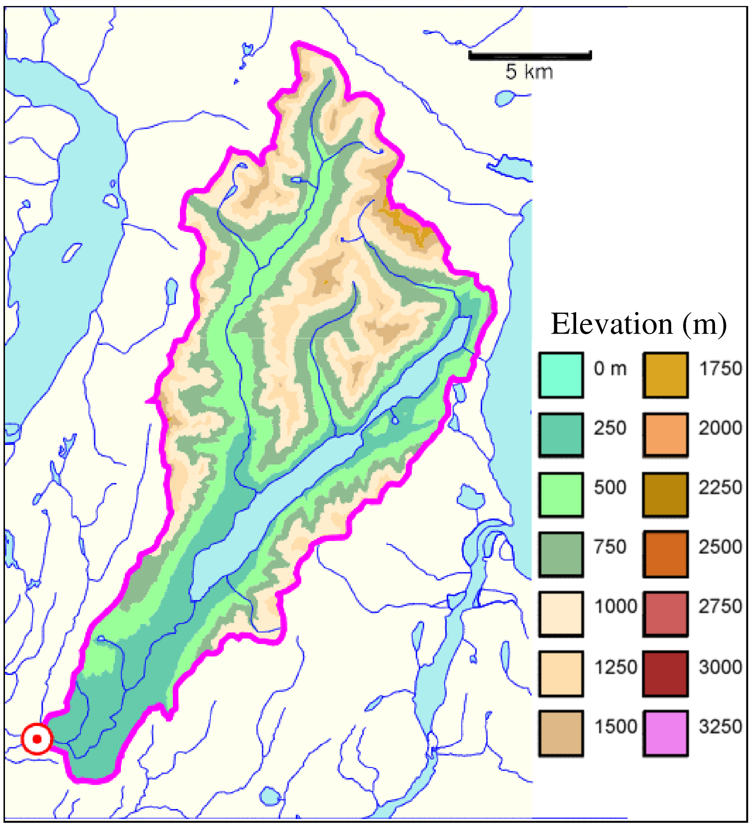

Figure 2: Alouette River watershed
(Water Survey of Canada 2009)

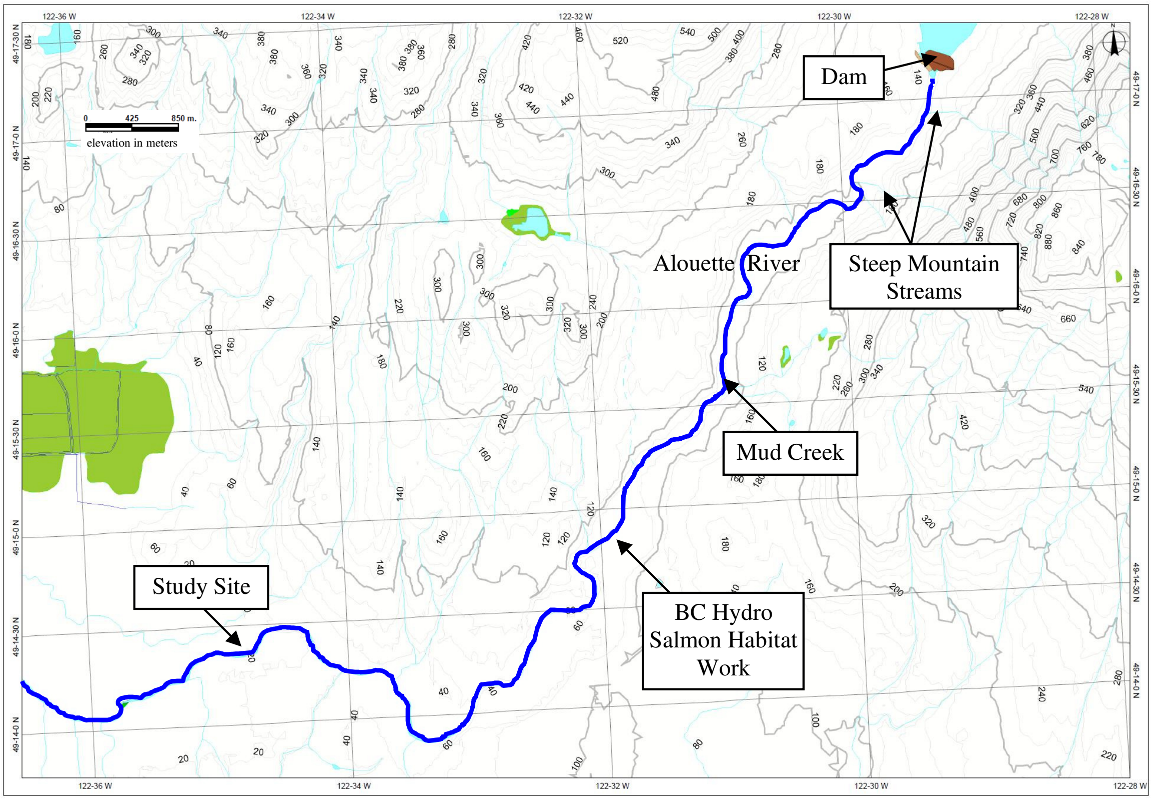

Figure 3: Alouette River study site and nearby reach


Figure 4: Alouette River photo from bridge looking upstream

The Alouette modeled reach starts at the bridge, about 50 meters downstream of the gauge, and runs 90 meters upstream. The channel has a riffle pool morphology with cobble bed, shallow pools and riffle spacing of 30-60 m. The channel curves into the study reach, forming a depositional gravel bar on the right bank and pushing the thalweg towards the left bank. The thalweg is paved with medium angular boulders, whereas the rest of the bed is covered with loose cobbles with gravel and sand on the banks and in the pools (see Figure 20). The clear-span bridge includes 500 mm angular riprap on both banks, but does not confine the flow, and the bed widens with an increased slope immediately downstream of the bridge providing a critical flow control for the gauge. There is a small secondary channel at the gauge that is active at high flows, and therefore it was included with the bridge riprap in the modeled reach (see Figure 5).

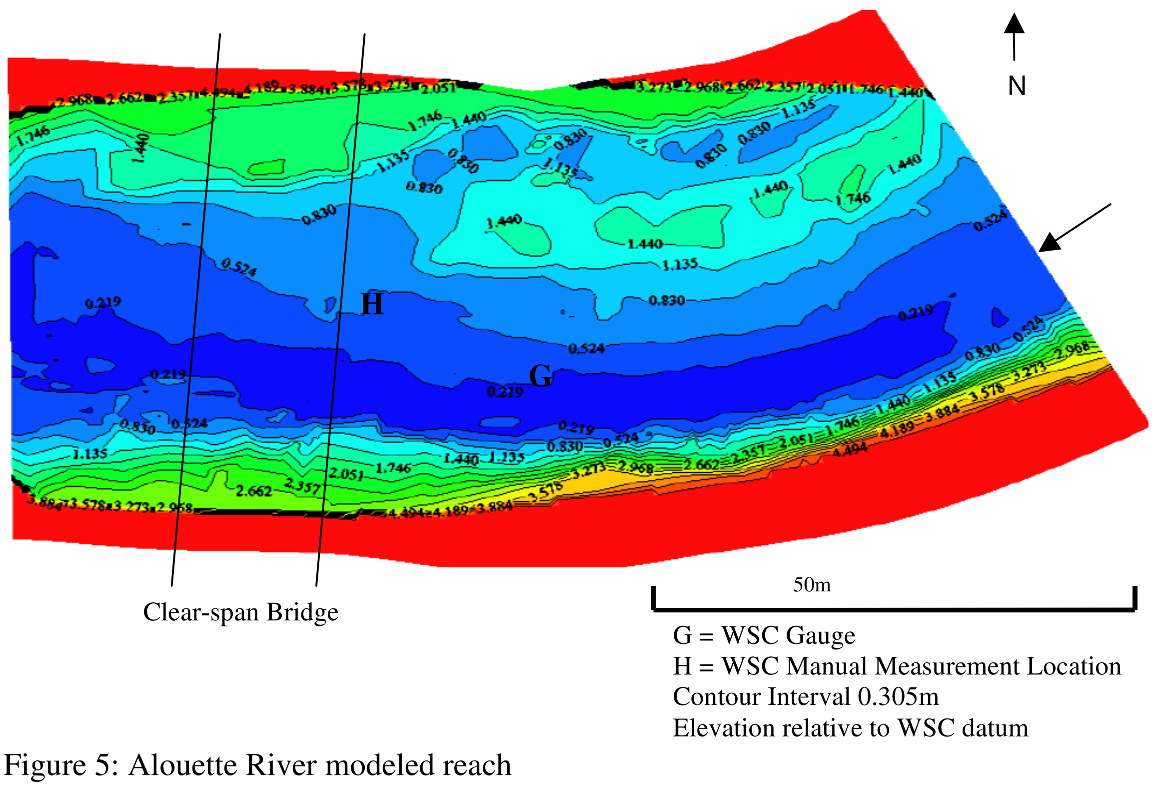

Figure 5: Alouette River modeled reach

Cayoosh Creek (WSC# 08ME002) is a coastal mountain stream with an 878 km^2 watershed, some limited glacial influence and a nival flow regime that typically peaks in June. Watershed elevations range from 340 m to 2700 m (see Figure 6). The land use is primarily alpine, subalpine, forest, and a few recent clearcuts (~ 6.5 %), and Interior Douglas-fir dominates the biogeoclimatic zone.

In 1979, a diversion located upstream of the field site was installed to divert up to 39 m^3/s during high flows with a mean value of 13 m^3/s. The diversion has a small pond and during the freshet the radial gates are periodically opened to drain the pond and flush a slug of sediment down Cayoosh Creek. The pond is also regularly dredged leaving a gravel supply imbalance that has resulted in coarsening of the bed material at the field site (Summit, 2002). Maximum and mean discharges of 211 m^3/s and 17 m^3/s, respectively, were recorded at the WSC gauge downstream of the diversion. The coarse gravel that by-passes the diversion accumulates in a 500m long depositional reach while the fine fractions move further downstream and eventually reach the study site.

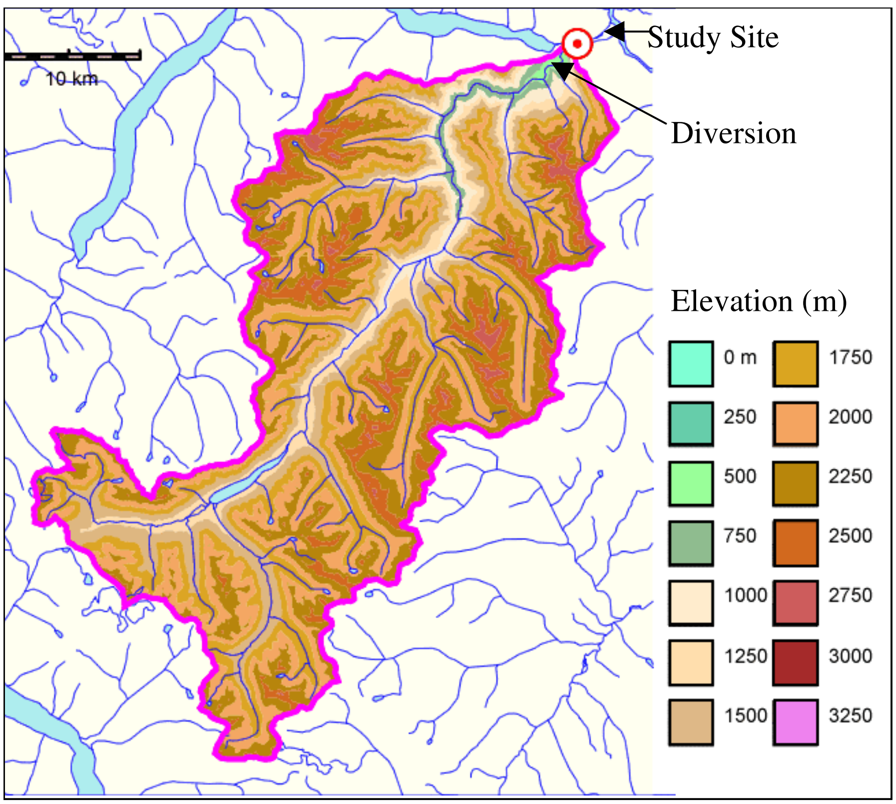

Figure 6: Cayoosh Creek watershed
(Water Survey of Canada 2009)

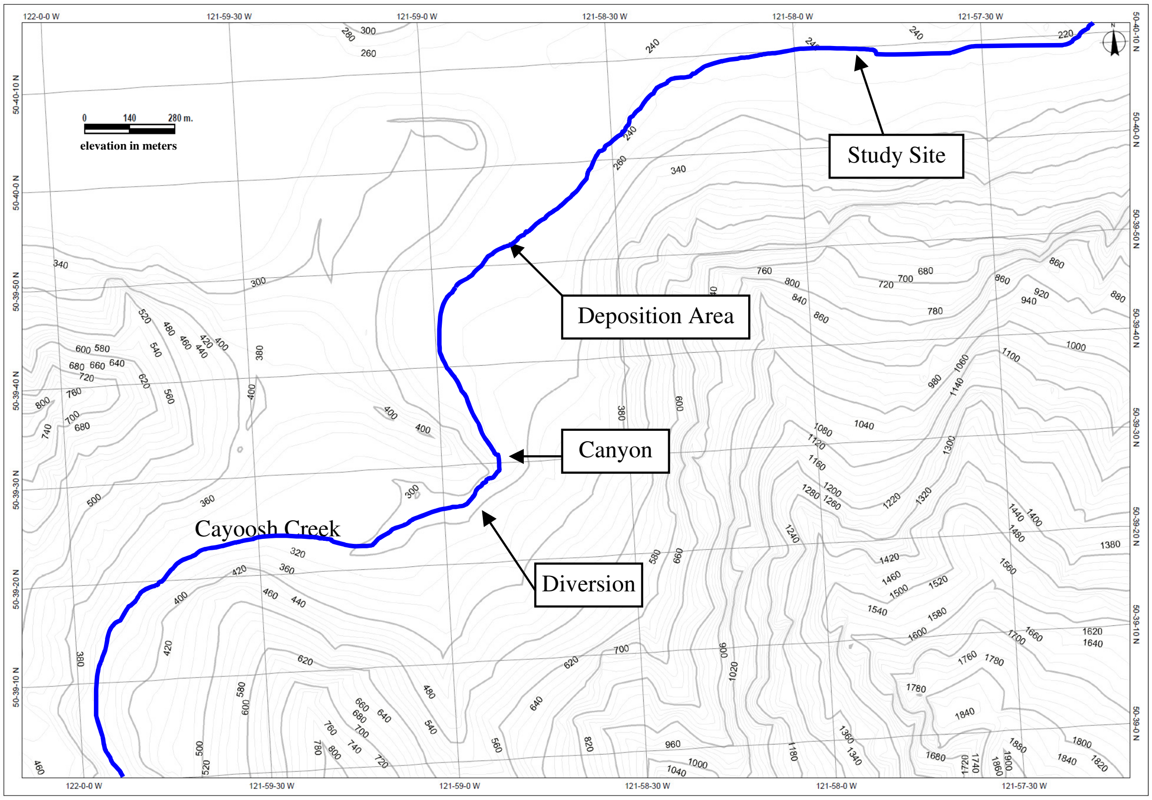

Figure 7: Cayoosh Creek study site and nearby reach


Figure 8: Cayoosh Creek photo looking downstream from bridge

The 210 m long study reach, starts about 20 m upstream of the gauge. A clear-span bridge immediately upstream of the study reach locally confines and deepens flood flows forming a stable scour pool on its downstream side within which the gauge is located. The above-mentioned coarsening has left a structured bed with large boulders over relatively subdued riffle-pool morphology and a shallow thalweg. The large boulders in the study reach could be relicts of glacial processes (e.g., non-fluvial) nonetheless, they control channel stability and resistance to flow. Bank erosion is an additional source of coarse material into the study reach. The creek has a short steep rapids section about 80 m downstream of the gauge station creating a critical flow control for the gauge and therefore was included in the modeled reach (see Figure 9).

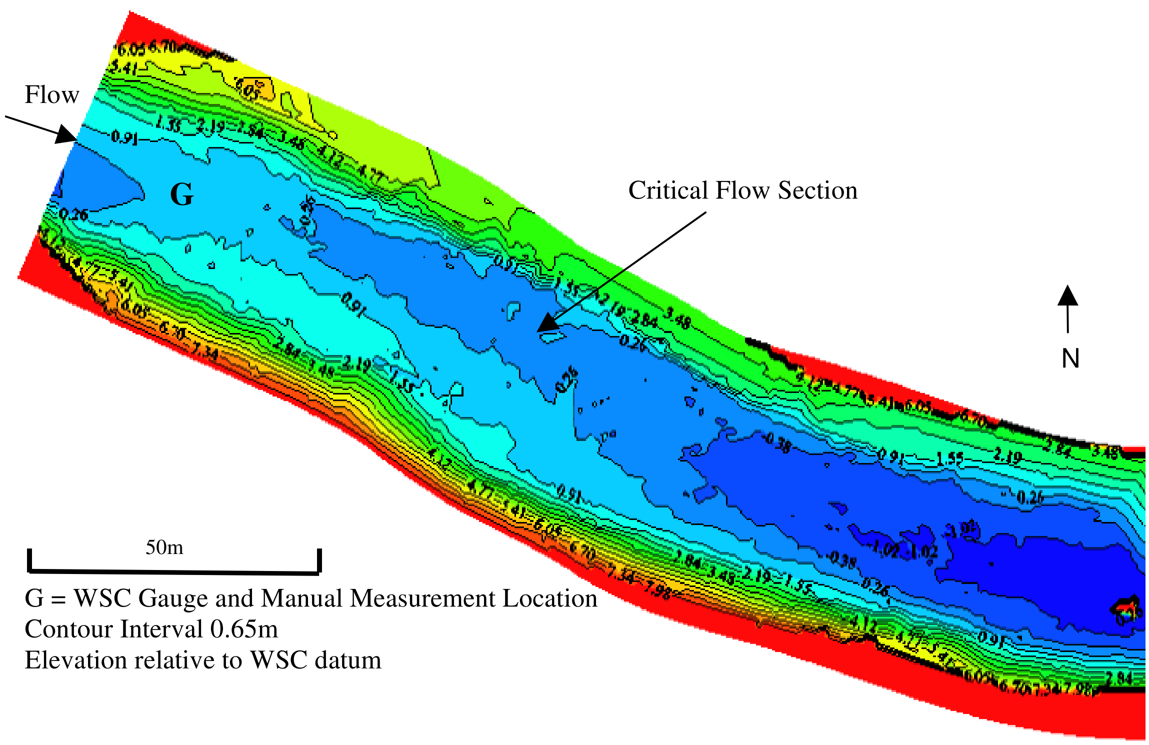

Figure 9: Cayoosh Creek modeled reach

The 1570 km^2 watershed of Baker Creek (WSC# 08KE016, 52°58" N, 122°31" W), is located in the interior plateau of BC and has a nival flow regime with a maximum and mean discharges of 129 m^3/s and 5 m^3/s, respectively. Watershed elevations range from

480 m to 1520 m (Figure 11). Young forest, clearcuts (~40%), agriculture and wetlands are the primary land uses in the watershed with Sub-Boreal Pine – Spruce,Sub-Boreal Spruce and Montane Spruce dominate the forest. Gravel sized sediment is provided by glaciofluvial colluvium along a deeply incised, meandering canyon that ends 2 km upstream of the field site.


Figure 10: Baker Creek photo looking upstream from bridge

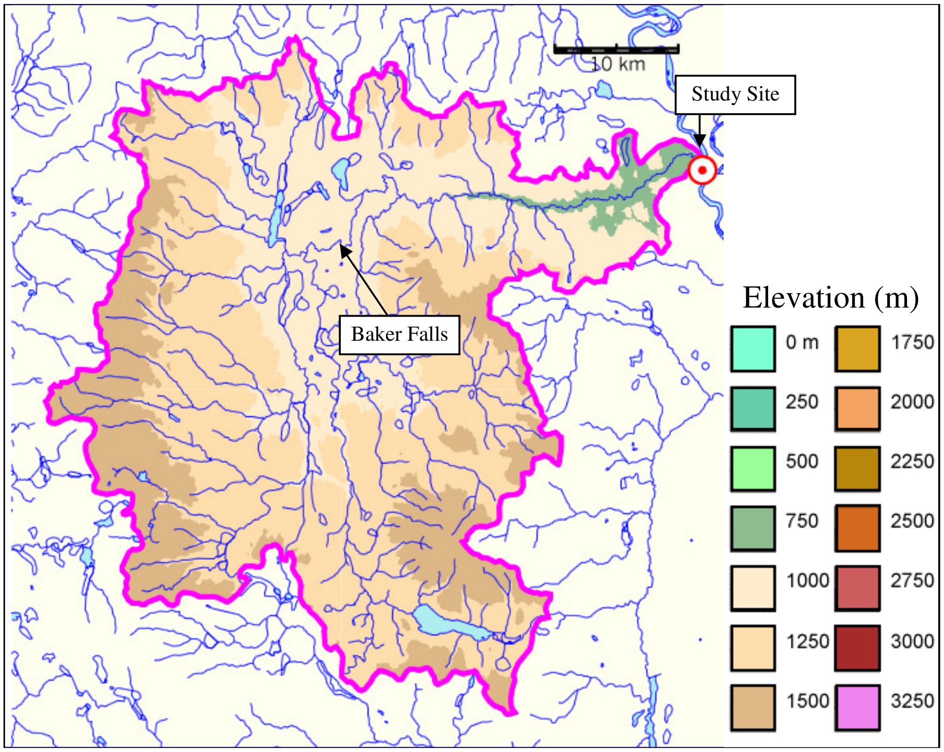

Figure 11: Baker Creek watershed
(Water Survey of Canada 2009)

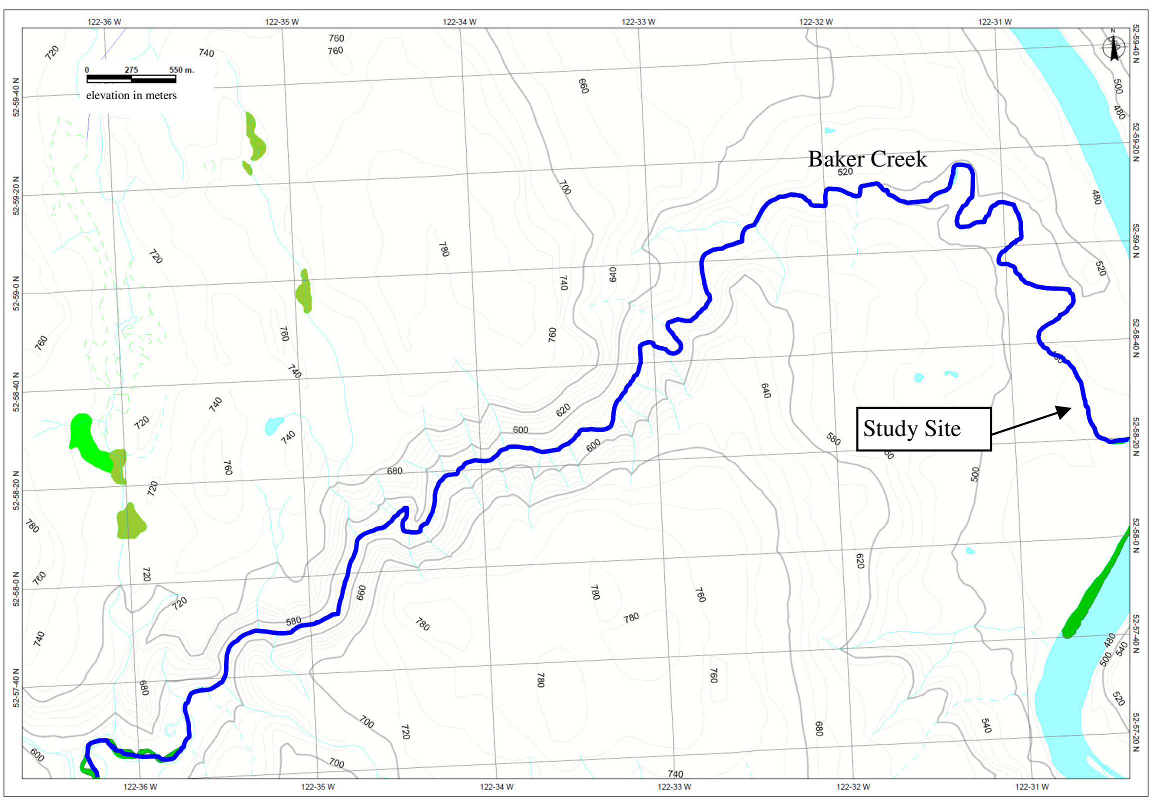

Figure 12: Baker Creek study site and nearby reach

The 206 m long study reach starts about 50 m downstream of the gauge (see Figure 13). A bridge narrows the creek downstream of the study reach with ongoing sediment deposition on the upstream side of the bridge causing a steep bed gradient and supercritical flow under the bridge. Therefore, the bridge acts as a flow control for the gauge and the flow was set to critical depth at the downstream end of the model. The channel thalweg crosses the channel from right to left bank and is paved with angular boulders. The right bank has riprap at the upstream end transitioning to cohesive sediments with roots at mid reach, and to gravel and silt at the downstream end, whereas the left bank consist of gravel filled in with silt and sand.

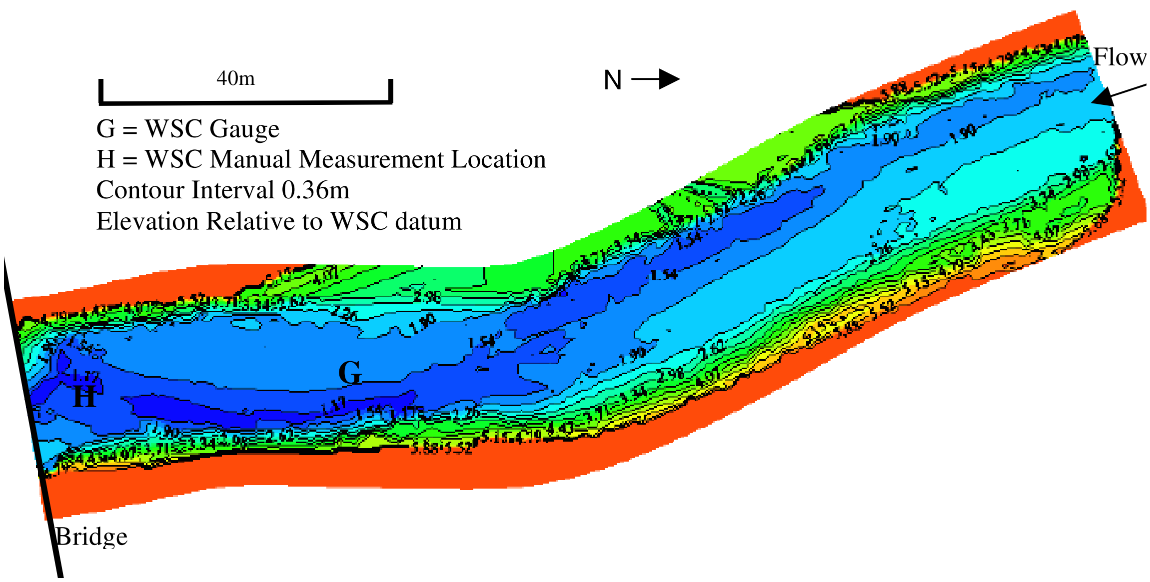

Figure 13: Baker Creek modeled reach

Finally, East Creek is located in the UBC Malcolm Knapp Research Forrest (49°16” N, 122°34” W), and is used for ongoing monitoring of sediment transport and channel morphology of a small mountain stream (Oldmeadow and Church, 2006; Caulkins and Hassan, 2007; and Hassan et al., 2009). The bed topography along ~300m of the study reach has been regularly surveyed every year since 2003, bedload traps and gravel tracers are used to measure sediment transport. The creek has a mobile bed, a 1.17 km^2 catchment, and mean annual and maximum discharges of 0.09 m^3/s and 2.6 m^3/s, respectively. The region has a maritime climate with wet mild winters and warm dry summers and the entire watershed is a Coastal Western Hemlock biogeoclimatic zone. Streamflow responds rapidly to rainfall and periods of low flow dominate during the summer months (Scordo and Moore 2009).

The upper portion of the creek is relatively steep, dominated by step-pool morphology. The gradient then flattens across a sediment wedge immediately upstream from a culvert through which the passage of cobbles is restricted (Oldmeadow and Church, 2006). Sand and gravel pass through the culvert and are measured using two sediment traps before being returned to the creek (Caulkins and Hassan, 2007). Immediately downstream from the culvert is a deep plunge pool followed by a long channelized section with average gradient of 0.020 and a rapids then riffle-pool morphology. The upper most part of the monitored reach, upstream of the modelled reach, is narrow and the channel is incised into old glacial till with large material. The till is the source of cobbles and boulder sized sediment and the study was carried out along 290 m meters of the riffle-pool portion of this reach (Figure 15).

Figure 14: East Creek photo looking downstream.
(Photo by J. Caulkins)

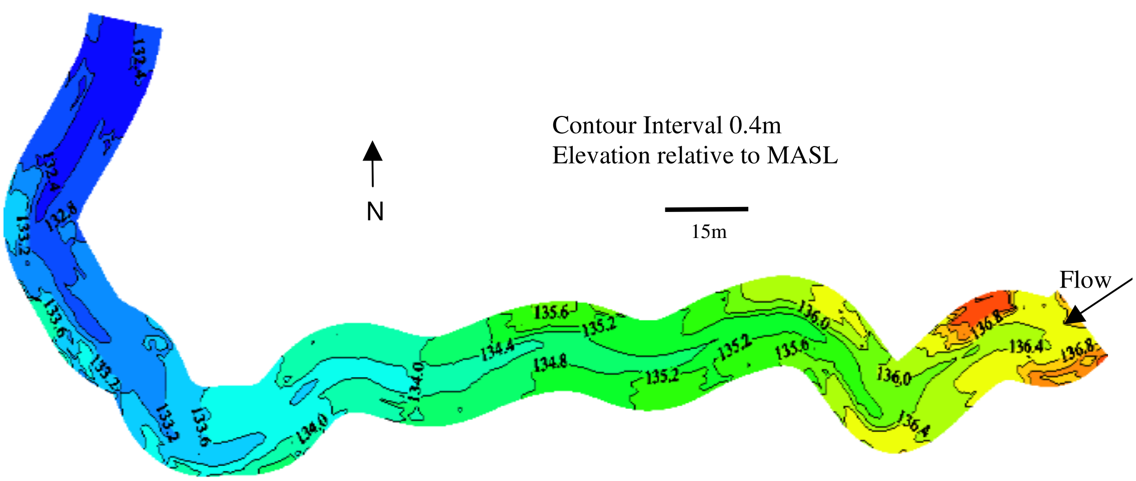

Figure 15: East Creek modeled reach

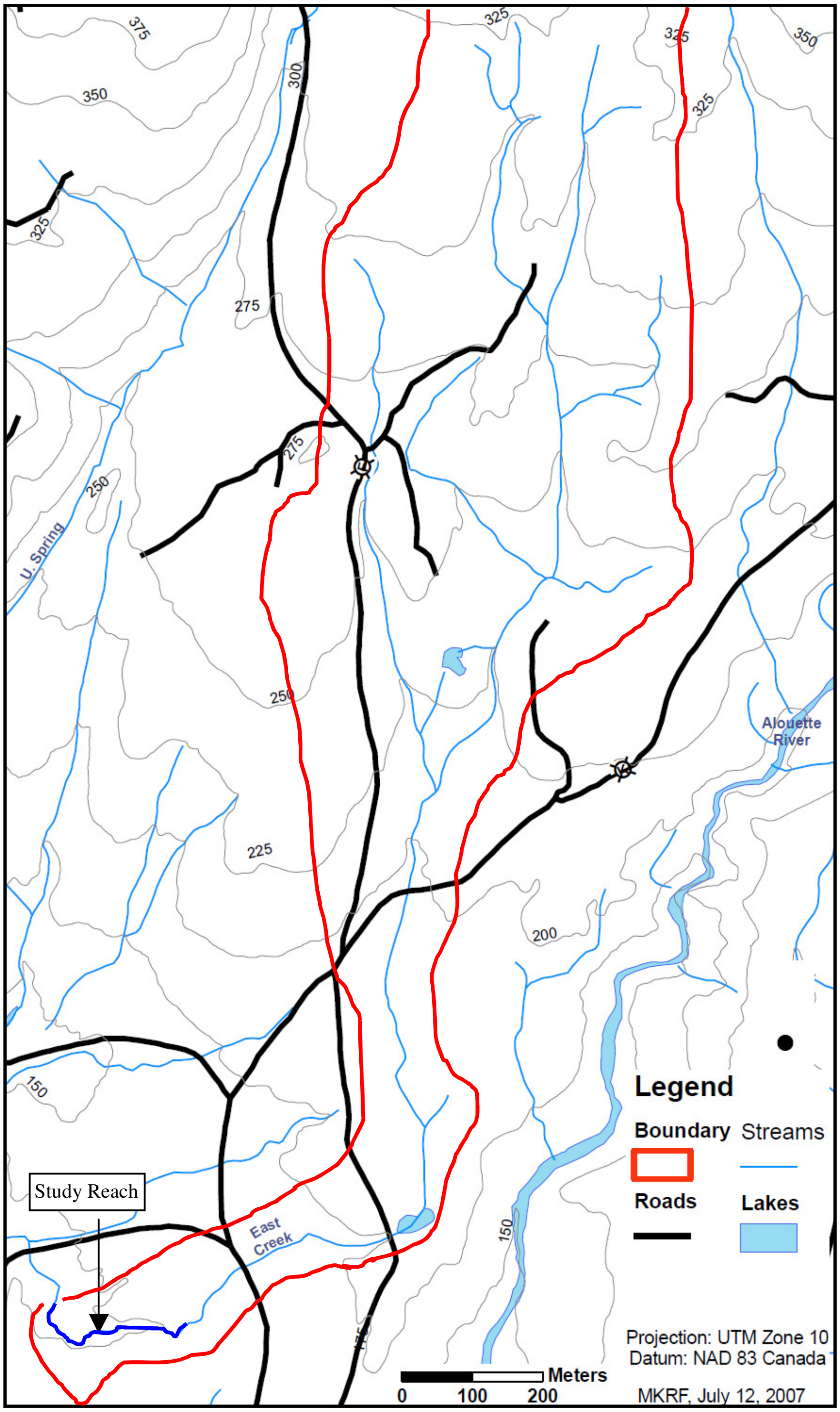

Figure 16: East Creek watershed

4 METHOD

The method can be separated into the numerical and field components and is presented in Figure 17.

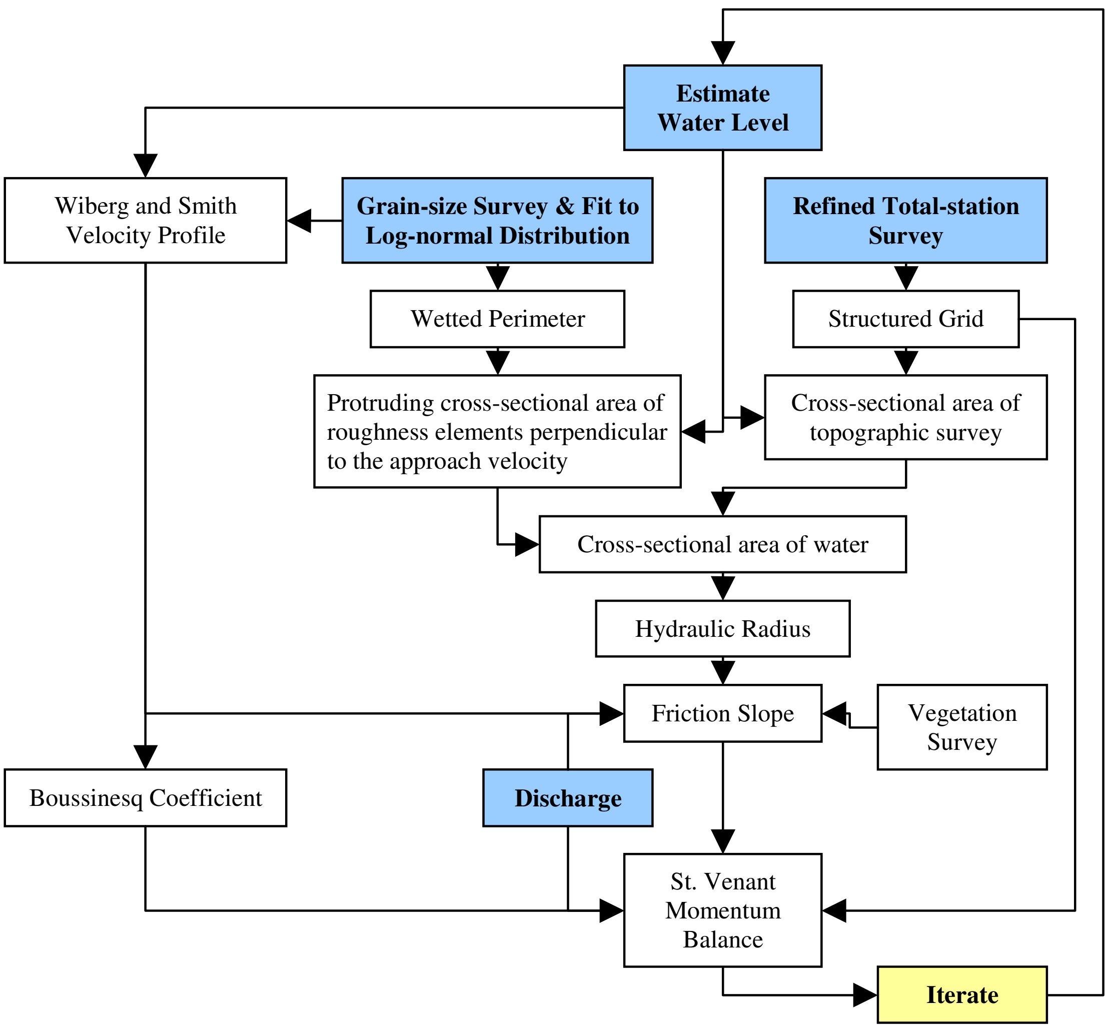

Figure 17: Method flow chart
(Blue boxes are initial inputs)

4.1 Numerical Model

In shear stress equations the flow depth, flow area and wetted perimeter variables are often not clearly defined (Smart, 2001) because they are typically calculated from channel surveys and are not related to bed roughness. Our topographic survey has spacing

1-2 orders of magnitude larger than the D_{50} grain size that forms the bed and therefore the three geometric parameters need to relate to both the macro-scale topographic survey and the micro-scale roughness survey. This is particularly necessary for spatially-variable roughness, where the vertical velocity profile is calculated locally and is more sensitive to macro-scale averaging of these parameters.

Kean and Smith used standard calculations of the wetted perimeter (P_{topo}) and cross-sectional area of flow (A_{topo}) based on the topographic survey. For this study three new formulae were derived to calculate cross-sectional area of water (A_{flow}), depth of flow (h_{flow}), and wetted perimeter (P_{flow}) that are based on the local sediment distribution derived from the roughness survey (Figure 17), and the hydraulic radius was calculated from P_{flow} and A_{flow}. See Appendix A for the derivations.

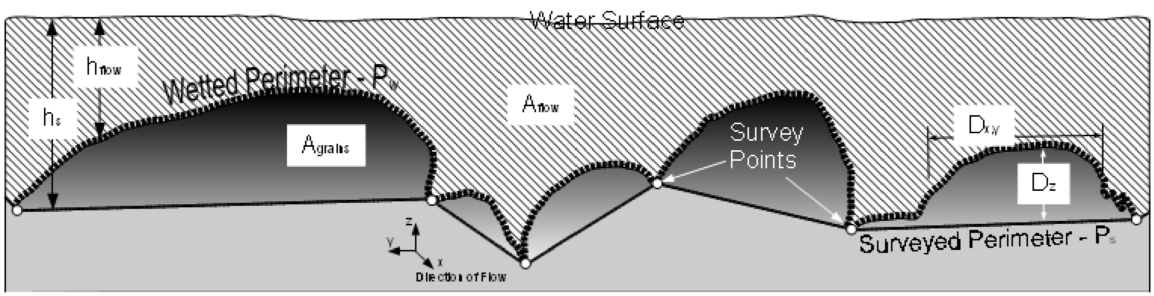

Figure 18: Visual depiction of the geometric parameters used in the study

Calculating the exact wetted perimeter depends on measurement resolution (Mandelbrot, 1967) which is limited by the steps between the size classes of the Wolman (1954) pebble count. The model uses a structured grid and each cross-section is divided into subsections (i) of roughly equal width (B_i). Assuming no stacked grains (Wiberg and Smith, 1991), the P_{flow} for each subsection (P_i) was calculated using equation (7).

$$P_i = \frac{\sqrt{(B_i)^2 + \left(h_{topo,i} - h_{topo,i+1}\right)^2}}{2\sum_{m=0}^{M} D_{z,m,i} c_m} s_1 \left[\sum_{m=0}^{M} D_{z,m,i} c_m - \sum_{m=where D_z > h_i}^{M} \left(D_{z,m,i} - h_{topo,i}\right) c_m \right] \tag{7}$$

The probability (c_m) is a discrete version of the log-normal distribution (Wiberg and Smith, 1991) for the individual grain-size classes ($D_{z,m}$) and s_1 is a shape factor. The grains were assumed to have a parabolic shape (Smart et al., 2004), therefore s_1=2.96. As the roughness parameters were mapped, the topographic surveyed depth (h_{topo}) was calculated as the distance from the water surface to the topographic survey elevation, and the total P_{flow} was determined for each cross-section as $\left(P_{flow} = \sum_i P_i \right)$. Equation (7) also assumes that the centres of the representative grain-sizes (D_m) are in a line along the cross-section and while this is false, and could result in a positive bias in the wetted perimeter, it is believed to be offset by the assumption that the grains are not stacked.

The Wiberg and Smith (1991) assumption of no flow blockage by grain particles is "potentially the most important effect that is neglected by the model" (Carney et al., 2006). For high relative roughness conditions a traditional survey could not accurately portray the flow pattern between boulders. To better represent the impact of large roughness elements on the flow, the field survey mapped only the low points between the boulders (Figure 18) and the expected protruding cross-sectional area of the bed roughness perpendicular to the approach velocity $\left(\overline{A}_{grains}\right)$ was calculated and added above the survey plane. This in turn restricted the cross-sectional area of water (A_{flow}) and helps accounts for flow blockage. $\overline{A}_{grains}$ was determined from equation (8) and subtracted from the cross-sectional area of the topographic survey (A_{topo}) to calculate A_{flow} in equation (9).

$$\overline{A}_{grains,i} = \frac{\overline{A}_{D,i}}{\theta_i} \tag{8}$$

$$A_{flow} = \sum_i A_{topo,i} - \overline{A}_{grains,i} \tag{9}$$

θ_i is the proportion of the subsection width (B_i) taken up by the width of one average grain, which is similar to the blocking ratio described by Smart et al (2004). $\overline{A}_{D,i}$ is the cross-sectional area perpendicular to the approach velocity of an average single grain. An estimate of the submerged boulder area, for each subsection of the cross-section, was calculated using equation (10).

$$\overline{A}_{grains,i} = \frac{B_i \pi}{4\sum_{m=0}^{M} D_{z,m} c_m} \left[\sum_{m=whereD_m \le h}^{M} {D_{z,m}}^2 {c_m}^2 - \sum_{m=whereD>h}^{M} \left({h_{topo}}^2 - 2D_{z,m} h_{topo} \right) {c_m}^2 \right] \quad (10)$$

The flow depth can be derived as a function of the cross-sectional area of water (equation (12)).

.

$$A_{flow} = \int h_{flow} dy \quad (11)$$

$$h_{flow,i} = h_{topo,i} - \frac{\pi}{4\sum_{m=0}^{M} D_{z,m,i} c_{m,i}} \left[\sum_{m=whereD_m \le h}^{M} {D_{z,m,i}}^2 {c_{m,i}}^2 - \sum_{m=whereD>h}^{M} \left({h_{topo,i}}^2 - 2D_{z,m,i} h_{topo,i} \right) {c_{m,i}}^2 \right] \quad (12)$$

To restrict the model results to gradually varying flow the critical depth was calculated and used as the lower boundary of the stage solution. Since each cross-section in the structured grid is discretized into multiple subsections with multiple depths and discontinuities in area. Numerically this leads to more than one local minimum in the specific energy of flow and hence more then one numerically calculated critical depth (Traver, 1994, and Chaudhry, 2008). To achieve a single 'critical depth' for a cross-section Traver (1994) calculated depth-average velocities for each subsection (i) of the cross section using Manning's n. Alternatively, Kean and Smith (2005) calculated an average critical Froude number (Fr) for the entire cross section by solving equation (13) for the critical water surface elevation ($WS_{critical}$) using the bed elevation for each subsection (z_i).

$$Fr = \frac{Q}{A_{topo}\sqrt{gR_{topo}}} = \frac{Q}{\left(\sum_i \left(WS_{critical} - z_i \right) B_i \right) \sqrt{gR_{topo}}} = 1 \quad (13)$$

However, an average Froude number does not account for the spatial variability of the flow across the channel and effectively interpolates the non-linear cross-section as a box culvert with area and height of A_{topo} and R_{topo} respectively. In this study, the critical depth was determined by assuming that Fr is critical at all points in the cross-section, preserving much of the cross-sectional shape, and the water surface elevation was calculated using equation (14).

$$Fr = \frac{Q}{\sum_i \sqrt{\left(WS_{critical} - z_i\right)^3 B_i^{\,2} g}} = 1 \tag{14}$$

The St. Venant equations were solved for the water slope by specifying the downstream stage to the critical depth. Alternatively Kean and Smith (2005) specified the water slope and solved the equations for the stage. The modeled stream reaches included the 'control', where the model typically calculated critical depth, and hence, the downstream stage provided negligible influence on the modeled stage height. If there had been backwater conditions then the critical depth assumption would not have been fulfilled and a two-stage model (Schmidt and Yen, 2008) or a variable slope model (Kean and Smith, 2005) would need to be used.

The numerical model was solved using the Newton-Rhapson iteration technique (Pappenberger et al., 2005) in a simultaneous solution procedure (Chaudhry, 2008). The program was coded in FORTRAN and the derivatives were discretized using a second order Taylor series approximation. Multiple channels were accommodated through the use of subsections. Each cross-section was divided into discrete subsections containing roughness parameters and a bed elevation unique to that subsection. The velocity profile was calculated and integrated for each subsection, and the individual values for the subsection discharge, area and wetted perimeter were summed for the entire cross-section. This provides a single node of information for each cross-section within the 1D model and multiple channels retained their own flow depths as well as Boussinesq and Chezy coefficients.

The Wiber and Smith (1991) velocity profile algorithm required iteration to derive the flow field (u/u_*) at any point in the water column, and the flow field was integrated over the depth and used in equation (5) to calculate the Chezy coefficient. When applied in a spatially-variable manner, this method involves a dozen iterations at thousands of locations for each step in the Newton-Rhapson procedure and hence the numerical approach is not computationally efficient, which is likely why it has not been widely used.

4.2 Field Surveys

Since the resolution of the stream-bed topography controls the performance of the numerical models (Pappenberger et al., 2005; and Hardy, 2008), separate surveys were conducted to measure the channel shape and the bed surface texture. Channel shape and surface texture surveys have typically involved simple mapping of the bed using a total-station and a single spatially averaged measurement of the roughness. However, this introduces elevation uncertainty at the same scale as the roughness elements, which can be significant for large roughness, and can be exacerbated by spatially-variable roughness elements.

To improve the channel survey resolution, a theodolite-based total station was used and only the local minimum elevations between the bed particles were measured. This enabled the direct estimation of the roughness and its superimposition on the mapped bed (Figure 18). Such a method resolves the Wiberg and Smith (1991) assumption that the bases of the bed particles all rest on a collective plane by establishing a realistic datum for the sediment. The survey spacing averaged one survey point per 1.2 m^2 for Alouette, per 2.25 m2 for Cayoosh and Baker, and per 0.25 m2 for East Creek.

Bed surface texture was determined using the Wolman pebble count (Wolman 1954). Where the bed was dry photographs were also taken of the sediment and analyzed using 'gravel-o-meter' software. For large scale roughness, such as boulders and steps, a bedform profiler (de Jong, 1995, and Smart et al., 2004), was used with 5 cm rod spacing. The profiler elevations were adjusted to remove the channel shape, and separated into individual roughness elements. The maximum, mean and standard deviation were calculated from the heights of these pieces as shown in Figure 21. The profiler measured the vertical axis (D_z) and the Wolman pebble count measured the intermediate axis (D_x). Following Wiberg and Smith (1991) it was assumed that

$$D_x = 2D_z \tag{15}$$

Where the water was too deep for a Wolman pebble count, the photo software, or the bed profiler, the maximum diameter was measured, the mean was estimated and the standard deviation was calculated as one third of the distance from the estimated mean bed level to the tops of the largest boulders (Smart, 2001). For large roughness, a second topographic survey was completed that measured the elevation of the tops of the boulders and was compared against the main topographic survey to provide a check on the estimate for the maximum vertical diameters.

The vast majority of numerical models have assumed that bed particles are randomly distributed throughout the reach. This supports the use of a single, spatially-averaged roughness parameter, which simplifies the grain-size surveys and enables reach-scale flow resistance equations. Moreover, spatially averaged stream roughness can be calibrated from velocity measurements and the use of a resistance equation. However, simple spatial averaging trivializes the non-linear relationship between flow and roughness, and there have been limited attempts to incorporate spatially-distributed channel roughness into flow models (Aronica et al, 1998, Folk and Prestegaard, 2000, and Lisle et al., 2000).

An alternative to simple spatial averaging is to assume that local flow responds to local grain size requiring a spatial representation of the roughness throughout the reach. Therefore, morphologically similar areas (i.e., similar roughness) were surveyed, and mapped to the same structured grid used for the topography of the channel. This implies that every point in the topography grid included a corresponding maximum, mean, and standard deviation of the roughness height (Figure 19). This method requires more detailed survey notes, but necessitates only a marginal increase in survey time. Such spatial mapping also resolves the assumption of spatially-averaged roughness in the Wiberg and Smith (1991) model.

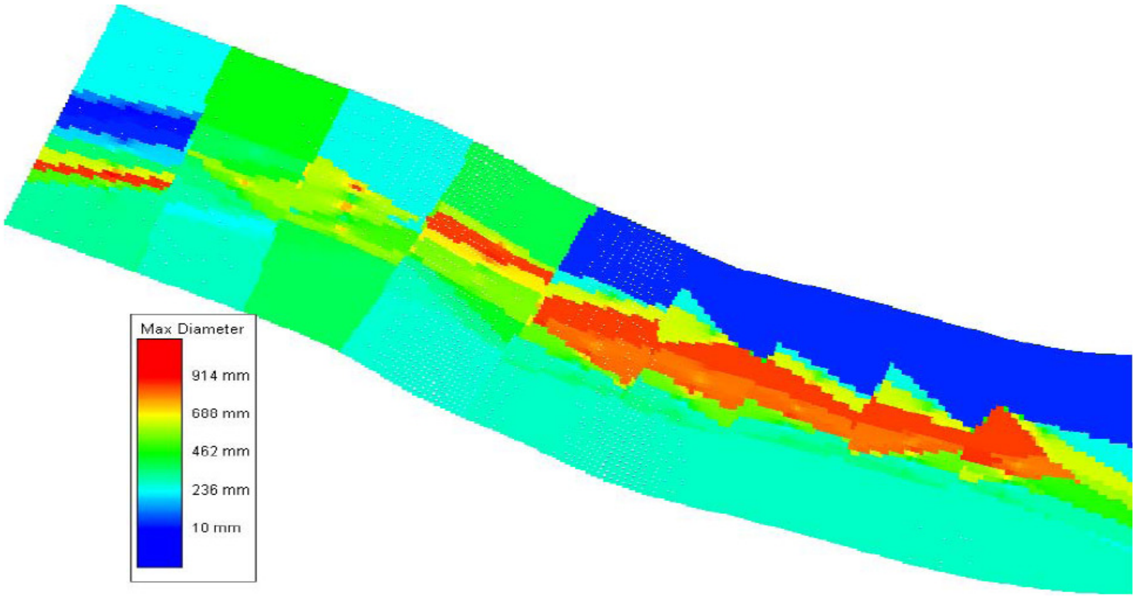

Figure 19: Sample of spatially-variable roughness data for the modeled reach of Cayoosh Creek.

To further exemplify the differences between the spatially-averaged and spatially-variable methods, the spatially averaged values of the maximum, mean, and standard deviation of bed surface texture are presented in Table 1. The flow model was re-run for the sites using these single spatially-averaged statistics (see results). For comparison and in order to illustrate the differences between the methods, the spatially-averaged grain-size distribution and the range of obtained distributions are presented in Figure 20.

Table 1: Spatially-averaged grain-size statistics.

	Alouette River	**Cayoosh Creek**	**Baker Creek**	**East Creek**
Max Diameter ($D_{x,max}$)	696 mm	980mm	500 mm	512 mm
Phi Mean ($\overline{\phi_x}$)	-5.53 (46 mm)	-5.59 (48 mm)	-5.22 (37 mm)	-5.34 (41 mm)
Phi Standard Deviation (σ_{ϕ_x})	1.92	1.51	1.33	1.13

Notes: ($\phi = -\ln_2(D_x)$)

$\overline{\phi_x}$ was calculated as the arithmetic mean of the local phi-means.

σ_{ϕ_x} was calculated as the root-mean-square of the local phi-standard deviations.

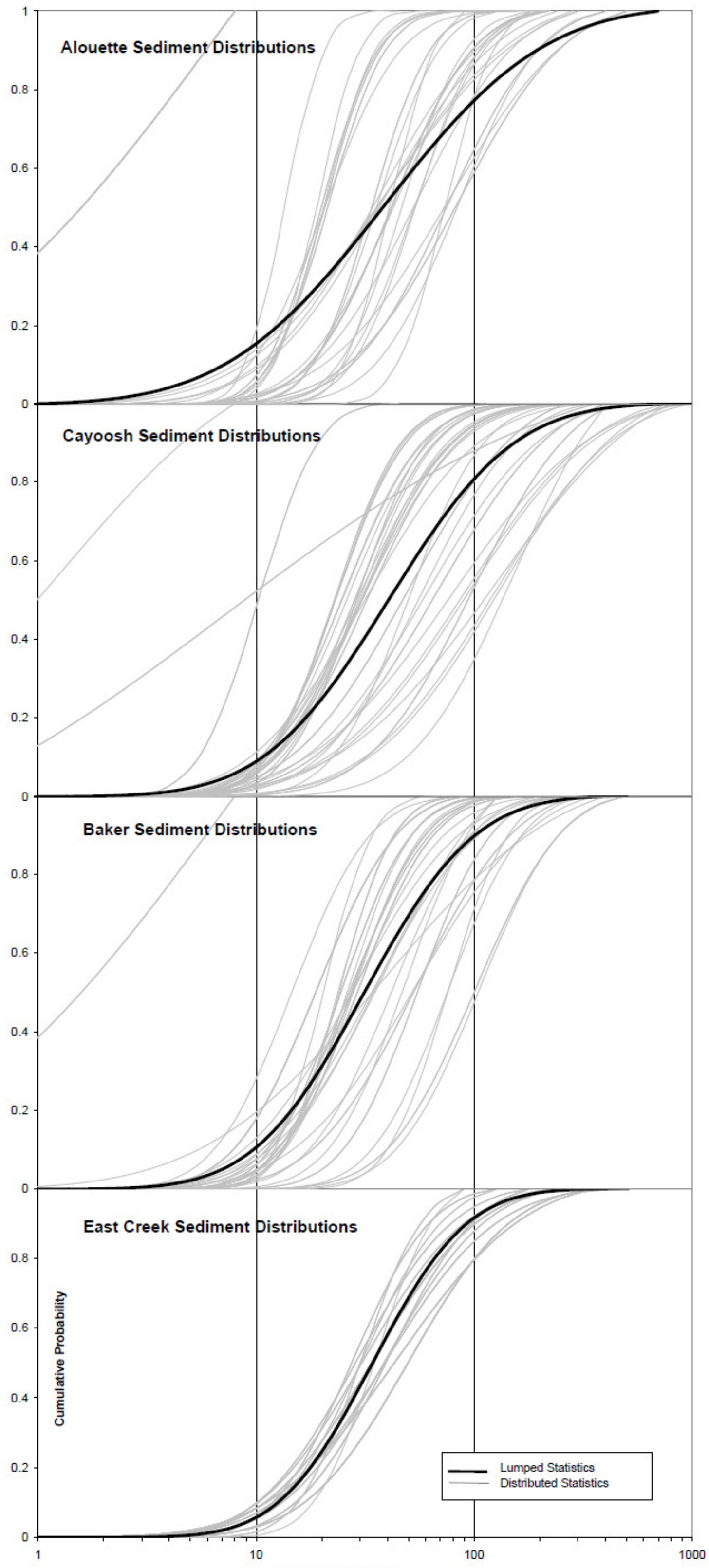

Figure 20: Comparison between the spatially-averaged and spatially-variable grain-size distributions.

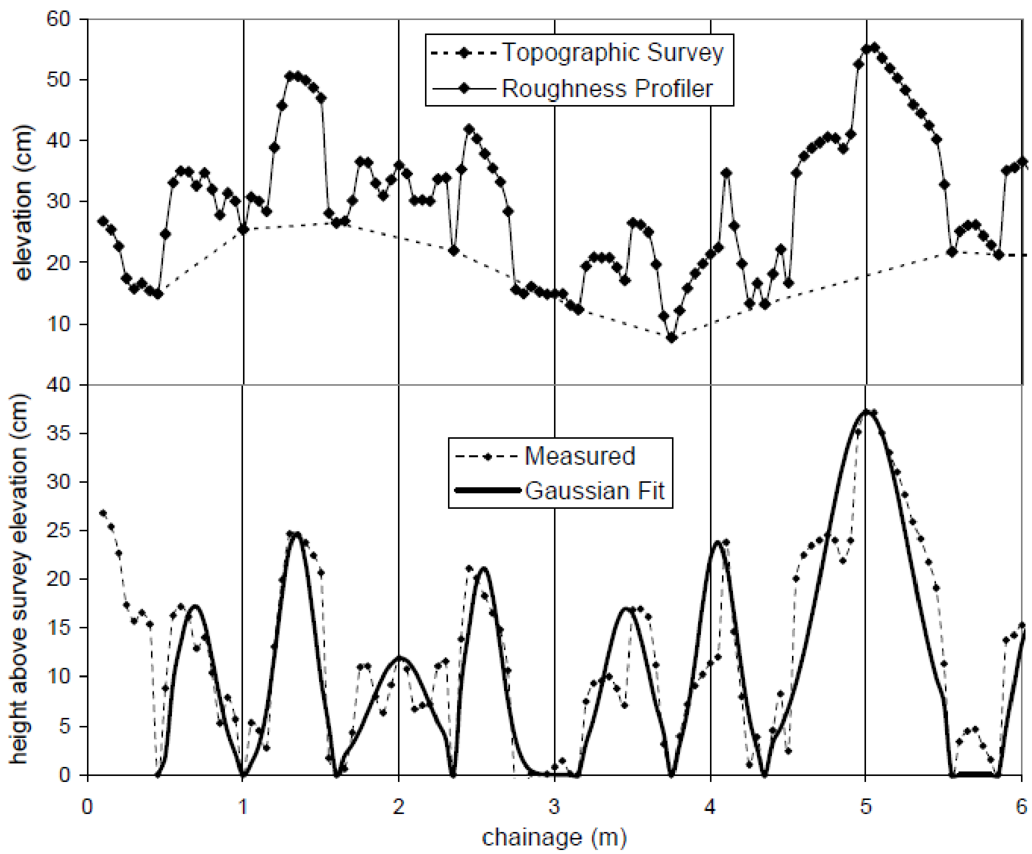

Figure 21: Gaussian fit of the measured stream roughness.

For East Creek the bed topography and sediment surveys were performed by several researchers over a period of six years. The roughness measurements at East Creek followed the Wolman pebble count method and the topographic surveys involved standard techniques, where the elevations were randomly measured regardless of sediment location. Given the relatively small grain-sizes of the sediment, the simple survey technique provided a small systematic bias in the modelling results. The error in stage is approximately equal to half the mean vertical height of the sediment (~ 12 mm) and is considered small.

The vegetation survey was conducted in a manner similar to that of Kean and Smith (2005), whereby areas of vegetation with similar diameter and stem spacing were mapped, then measured and averaged for the areas. The gathered vegetation information was implemented in a manner similar to that of the grain size.

5 MODEL RESULTS AND DISCUSSION

The modelled stage-discharge relations are compared against manually measured stages for specific discharges in Figure 22 through Figure 25, with uncertainty calculated as described by Herschy (1999), and the results are discussed in reference to the main assumptions. The Water Survey of Canada (WSC) measured the manual discharges for Alouette River, Cayoosh Creek and Baker Creek between 2007 and 2009 using the velocity-area method (Herschy 2008). The locations of the WSC measurements, and where the results were extracted, is depicted by the H in Figure 5, Figure 9, and Figure 13.

The sites are presented in the order of their channel bed modelling complexity. Alouette has simple small-scale roughness, Cayoosh has large-scale roughness, Baker has a mobile bed, and East Creek has a mobile bed that is modelled over a period of years. The model for East Creek was run for each of the six survey years and, to highlight the effects of bed mobility (scour and fill) on the stage-discharge relation, curves for each survey year are presented for five cross-sections along the study reach. None of the model parameters were calibrated.

5.1 Alouette River

The modelled and measured discharges for Alouette River are presented in Figure 22. Lisle et al (2000) and Wiberg and Smith (1991) assumed the bed particles could be spatially-averaged, leading to a spatially-constant drag coefficient. Implicit in this assumption is that either the bed particles are randomly distributed or that the flow is not affected by positioning of roughness over the reach. Such spatially-averaged roughness may be adequate for relatively homogeneous bed morphology (Kean and Smith, 2005) but it consistently underestimated the stage at Alouette River (see Figure 22). Near bed shear stress and the vertical velocity profile adjust to changes in roughness in a complex and non-linear manner (Lisle et al., 2000, and Yen, 1999). A simple averaging of the roughness could obscure the non-linear force balance in the water column and bias the momentum balance.

In the Alouette reach, the finer sediment is located on the banks of the river and larger sediment located in the thalweg. When the grain-sizes were spatially-averaged, the mean sediment diameter was suppressed for the thalweg region, where the highest velocities are located, and the maximum sediment diameter was over estimated on the edges of each cross-section. This resulted in higher momentum in the deep central portion of the flow, lower momentum in the shallow outer portions of the flow, and overall a higher total momentum. Overestimating the momentum reduces the cross-sectional area of water needed to convey the flow and hence underestimates the stage.

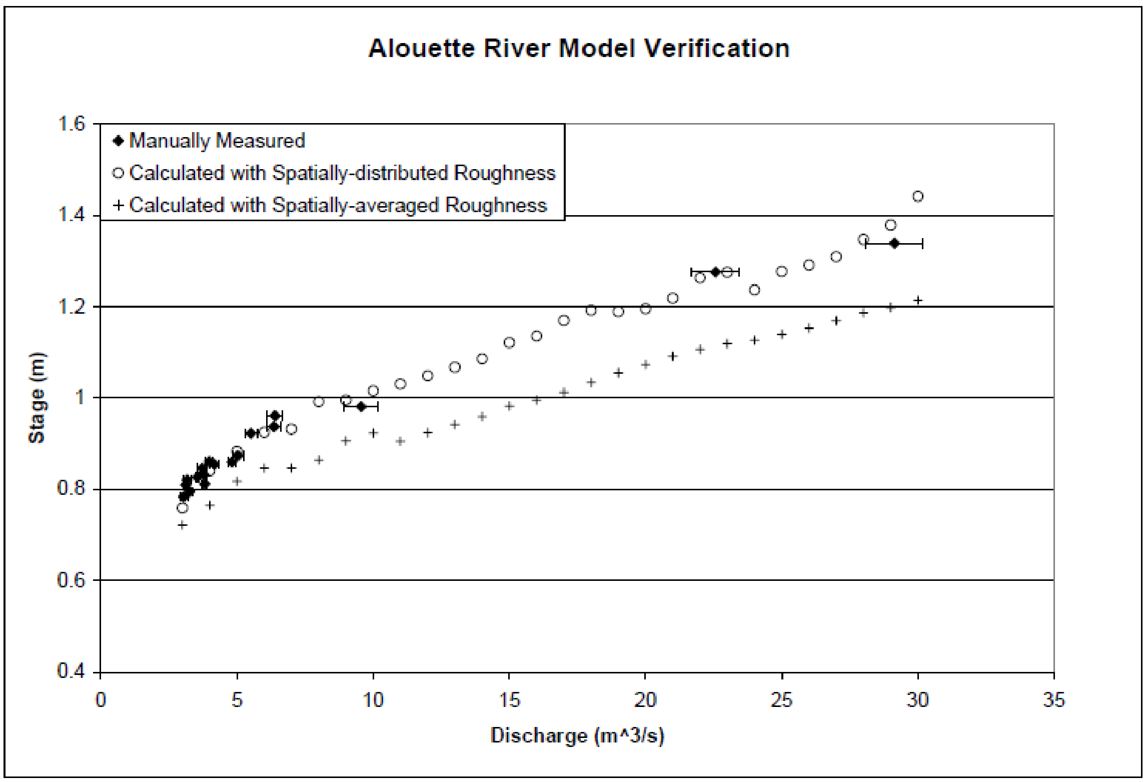

Figure 22: Alouette River model verification using measured data from

Errors in the survey measurements are considered small and random compared to the systematic functional error. Functional errors are a result of the reduction of the complex physics inherent in turbulent open channel flow into a discrete, one-dimensional set of equations with a detached and simplified roughness model. Freeman et al (1996) determined that the single most important source of error in stage-discharge modelling is within the roughness coefficient. Kean and Smith (2005) calibrated their roughness length to stage-discharge measurements, which likely helped to reduce the roughness error, while the roughness length was calculated from the grain size statistics for this study. Bohorquez and Darby (2008) varied the roughness length of a 1D momentum model to estimate the model error, and a Monte Carlo model (Pappenberger et al. 2004) could be used to assess the sensitivity of the roughness length on the model.

Because we used a 1D momentum model, additional functional error can arise when trying to model flows that incorporate significant two- and three-dimensional effects (e.g. secondary circulation, dispersion, and turbulence - Hardy, 2008). Two-dimensional stream models (Wilson et al., 2002) could alleviate much of the functional error and three-dimensional models (Jazizadeh and Zarrati, 2008) have the same number of dimensions as the underlying processes. Unfortunately this results in an increase in measurement error as additional dimensions require unrealistically fine spatial detail to define the roughness surface (Horritt and Bates, 2002), or to support additional roughness parameters (Hardy, 2008, and references therein). However, it would be worthwhile to evaluate the spatially-distributed roughness and new formulae for flow area and wetted perimeter within two and three-dimensional momentum models.

With the 1D model a sensitivity analysis should be done to determine the maximum survey spacing, as well as the corresponding structured grid spacing, needed for an accurate model, as there is a point where accuracy gained through additional survey measurements is negated by the functional error. It may be possible to reduce the number of grain-size measurements down to a handful of surveys, each of which runs along an estimated flow streamline, although streamwise sorting (Lisle and Madej, 1992) may negate any benefits.

5.2 Cayoosh Creek

For Cayoosh Creek, the modeled stage-discharge relation was calculated using three methods: 1) with spatially-variable roughness and using the Wiberg and Smith (1991) model for the velocity profile, 2) with spatially-averaged roughness and the Wiberg and Smith (1991) model, and 3) with spatially-variable roughness and the simple log-law model. All three models underestimate the stage for low flows by 0.2 m, while method 3 also underestimates the stage at medium flows (20-40 m^3/s) leaving the Wiberg and Smith model as the best estimate for stage at these flows. The mean annual flood for Cayoosh is 96 m^3/s but the WSC does not have any recent measurements higher then what is shown in Figure 23.

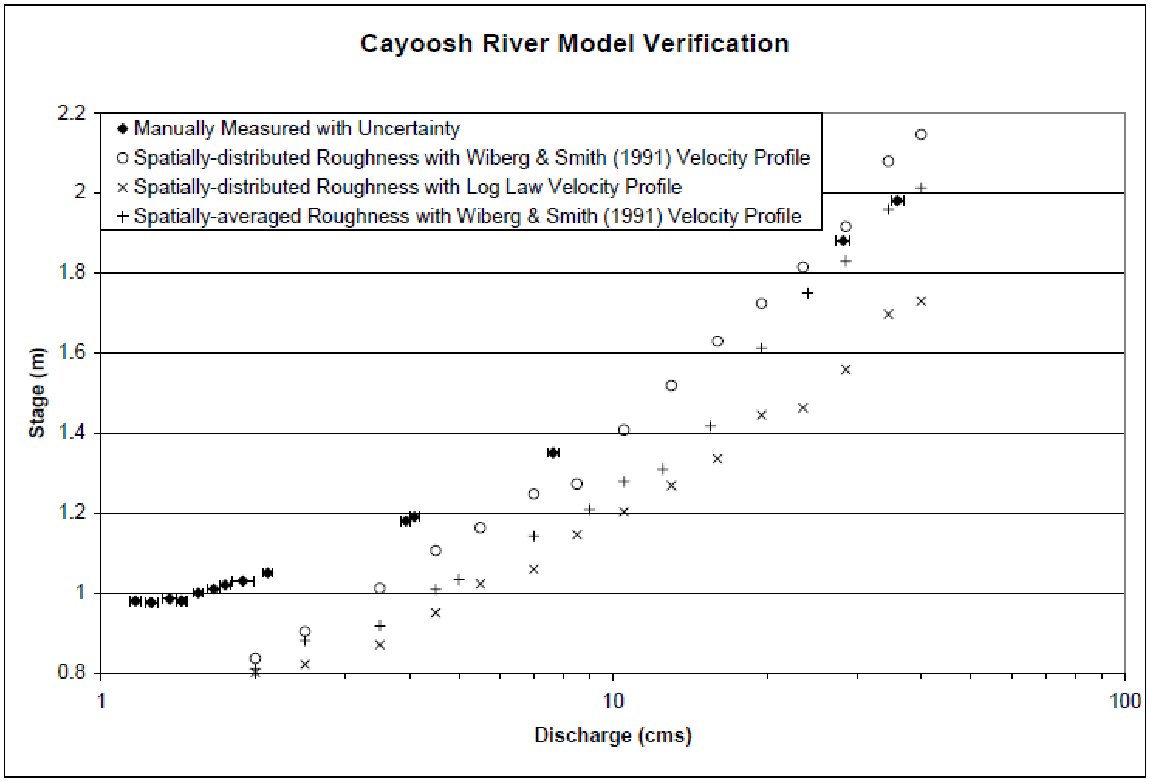

Figure 23: Cayoosh Creek model verification using measured data from

The low flow discrepancy is not believed to be the result of incorrect model datum, or bed movement prior to the survey. The low flows are controlled by a natural weir-like crest at the downstream end of the gauge-pool that had formed a riffle (see Figure 24). The bed material at the pool-crest is primarily boulders and sand and the funnelling of the water through the riffle, due to sediment imbrication, may have increased the upstream stage. The spatially-averaged distribution model consistently underestimated the stage at Cayoosh Creek, which is similar to the Alouette results although the difference is not as dramatic. The small difference is possibly due to the more spatially uniform grain size distribution at Cayoosh and the thalweg is not as pronounced as at Alouette.


Figure 24: Close-up of riffle at downstream end of the gauge-pool at Cayoosh Creek.

The large roughness model (Wiberg and Smith, 1991) significantly influenced both the Chezy and Boussinesq coefficients within the momentum calculations. The modifications to the Kean and Smith (2005) method helped address the Wiberg and Smith assumptions regarding flow blockage by sediment, grains not being stacked, and spatially-averaged roughness. Neglecting the shadowing effects of sediment in the streamwise direction may have the most impact on the current model since the cross-sectional area of water and wetted perimeter calculations only addresses the sediment geometry in the transverse direction. Additional roughness survey techniques such as sand spreading, laser scanning, low level aerial photography and line-by-number sampling have been used to estimate sediment imbrication (Smart el al., 2002, and Smart et al., 2004). Unfortunately most of these methods require a dry bed except line-by-number sampling, which may be complimentary to the methods used in this study. If the shadowing effect is quantified, it is uncertain how this could be incorporated into the Wiberg and Smith model. Alternatively sediment imbrication could be represented by a hiding functions (Parker, 1990), but combining it into the velocity profile model would also require further research.

Grain-size measurements at Cayoosh involved a combination of direct measurement of the vertical axis diameter and indirect calculation of the vertical axis from intermediate axis measurements. The Wiberg and Smith model assumes that $2D_z=D_{b\text{-}axis}$ and is supported by Green (2005). Comparisons were made between the vertical and intermediate axes of the grains and although the relation between the two could be roughly 2:1, there is a wide variation. This assumption could be resolved by measurement of only the vertical axis in the field, which eliminates the photo analysis technique but line-by-number sampling (Smart el al., 2002) could be used to provide an additional check. Also it may not be necessary to do full grain-size distribution analysis, when perhaps the distribution of the 10 largest grains, or the hybrid technique (Rice and Haschenburger, 2004), or the topsum technique (Clancy and Prestegaard, 2006) could formulate an accurate velocity distribution utilizing the Wiberg and Smith (1991) approach, and reduce the time spent surveying.

5.3 Baker Creek

Baker Creek is unstable relative to Alouette River and Cayoosh Creek. The stage-discharge relation for the gauging station at Baker Creek is dominated by the channel shape at the downstream bridge. This provides a critical flow control at all discharge levels, and therefore the choice of roughness distribution, spatially-averaged or spatially-variable, had no influence on the model results (Figure 25). The flood frequencies in Figure 25 were calculated assuming a Gumbel distribution. The model results are in good agreement with measured discharges for the 2008/09 water year, the same year that the survey was completed (Figure 22). However, there is a significant difference between the modeled and the measured stages for years prior to 2008. The manual measurements for Alouette River and Cayoosh Creek were below the mean annual flood, and hence the flood frequencies were off the chart in Figure 22 and Figure 23.

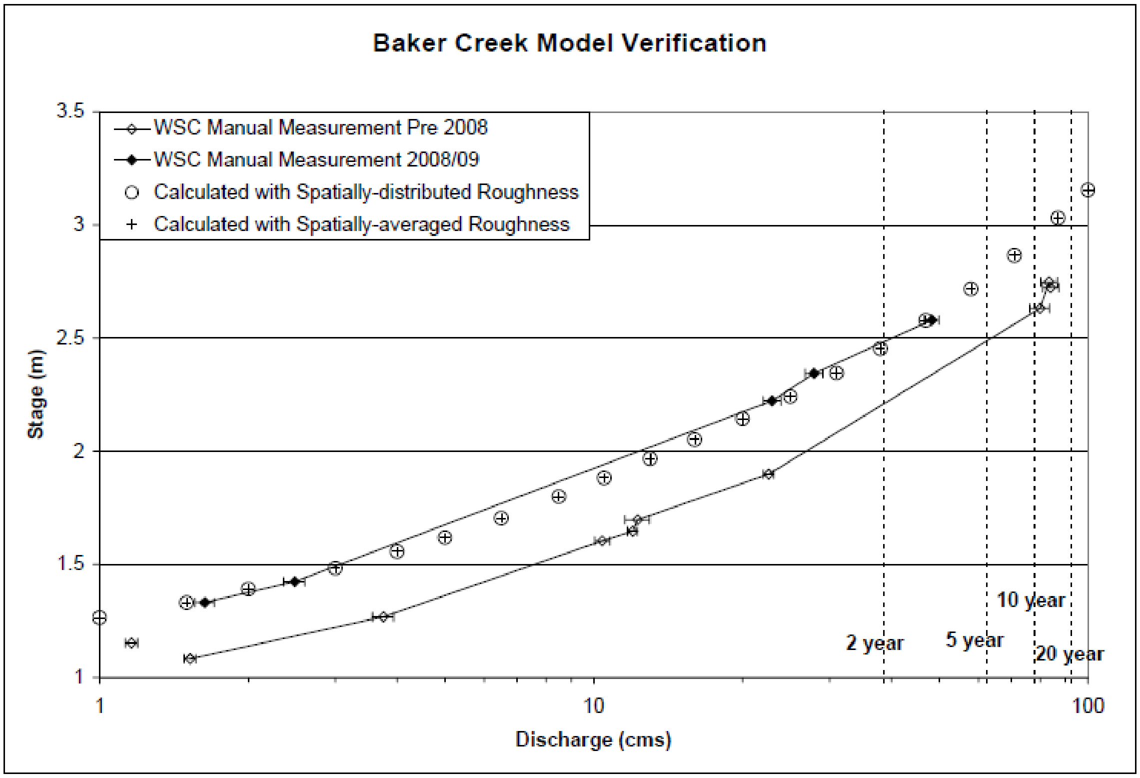

Figure 25: Baker Creek model verification using measured data
The measured values align closely with the calculated values for the year of the physical survey (June 2008 – April 2009). Significant bed movement occurred during the freshet in May 2008 and the model does not align with the values that were manually measured prior to 2008.

In May of 2008 the gauge site experienced a 50 year flood, which may have significantly altered the bed topography and stage-discharge relation. Piecewise linear stage-discharge relations before and after the flood suggest a shift from 6.8 m^3/s to 2.5 m^3/s for the 1.42 m stage (Figure 22). The two curves are roughly parallel when plotted in log space therefore the difference in discharge increases as the stage increases, resulting in a shift from 76 m^3/s to 48 m^3/s at the 2.58 m stage. This upward shift in the stage-discharge curve suggests there was a net sediment deposition at the gauge location and, as noted by Kean and Smith (2005), this type of model is not designed for unstable channels.

Baker Creek reinforces the fact that stage-discharge relations are dynamic (Dottori et al., 2009). Water resource managers often make decisions based on real-time discharge data, but adjustments to the relations, due to geomorphic change, continue to lag stage measurements by months and the changes are normally applied retroactively (Hamiton, 2009). There is a growing call for improved modelling to enable real-time adjustments of stage-discharge relations (DeGagne, 1996, Cao and Carling, 2002, Kean and Smith, 2005, Hardy, 2008, Dottori et al., 2009, and Juracek and Fitzpatrick, 2009), and the results from Baker and East Creeks contribute to this call.

5.4 East Creek

Following the Baker model, East Creek was subsequently modeled to demonstrate how the stage can shift in a mobile bed. The numerical model for East Creek calculated stages along the reach for six separate topography surveys taken over six years (2003 to 2008). The resulting stage-discharge relations for several specific cross sections are presented in Figure 26 and the corresponding cross-sections are presented in Figure 27. The pin numbers indicate the nearest established survey markers.

Figure 26-Pin#38 shows a location where the stage-discharge curve changed very little, possibly due to no change in the topography (see Figure 27). It demonstrates how a well-selected site could have very little change in the stage-discharge relation over time.

Figure 26-Pin #40 & #41 demonstrate the large changes in theoretical stage-discharge curves that occurred between years, with the most dramatic changes occurring in the winter of 2006/2007. Between 2004 and 2005 the discharge at pin #140 shifted from 1.2 m^3/s to 2.0 m^s/s for the same stage (134.60m). This was followed by shifts down to 1.55 m^3/s then up to 2.2 m^3/s at the same stage for 2006 and 2007, respectively.
The results for pin #146 were more dramatic, where the discharge went from 2.9 m^3/s to 0.9 m^s/s then to 0.4 m^3/s for the same stage (133.30m) over the years 2006, 2007 and 2008, respectively. Correlating this to flood peaks, East Creek experienced one bankfull event during the winters of ’03/’04 and ’04/’05, zero events in ’05/’06, and three bankfull events during the winter ’06/’07 (Caulkins, 2009). The corresponding cross-sections in Figure 27 do not show a large change between years as the bed shift changes occurred downstream of both locations. However there was significant bed shifts downstream of both sittes (Figure 28).

Figure 26-Pin #47 & #52 show modelled results for locations where there were large shifts in the upper or lower portions of the stage-discharge curve respectively, with small changes in the curves at the opposite ends. In Figure 26-Pin #52 the lower part of the stage-discharge curve could have shifted as a result of erosion (or fill) of the low water control, while the mid-stage and high-stage part of the bed may have retained the original shape. Hence at high water the high stages maintained the previous stage-discharge relationship when the influence of deposits (or erosion) on low-water control were drowned out. Thus the scour and fill of the low water control resulted in a series of stage-discharges that spread out fanwise at the low flows. The opposite may also occur where the low water control is stationary, due to armouring or bedrock, and there is deposition or erosion at the high levels during floods causing an opposite fan of curves (see Pin #47). The corresponding cross-sections in Figure 27 displays bed shifts on the banks and in the thalweg for Pin #47 and #52 respectively.

Figure 25 and Figure 26 illustrate how various different types of shifts in the stage-discharge relation may be necessary depending on the nature of the gauging location and bed movement. Following a channel mobilizing event conventional stream gauging requires a manual measurement of stage (h_{manual}) and discharge (Q_{manual}) to determine the bias (Δh) in the old stage-discharge relation at Q_{manual}. Then one or more portions of the stage-discharge relation are adjusted. The adjustment is primarily a shift in the relation at Q_{manual}, where the shift may be equal to or less than Δh. There are also secondary shifts in the relation for discharges that are higher and lower then Q_{manual}, but those secondary shifts may be equal to Δh at all discharges, or may be weighted by previous manual measurements, or may be weighted by the magnitude of the discharge along the curve. This leads to many different ways in which a relation can be adjusted, the effectiveness of which depends on the skill and intuition of the hydrographer (DeGagne et al., 1996).

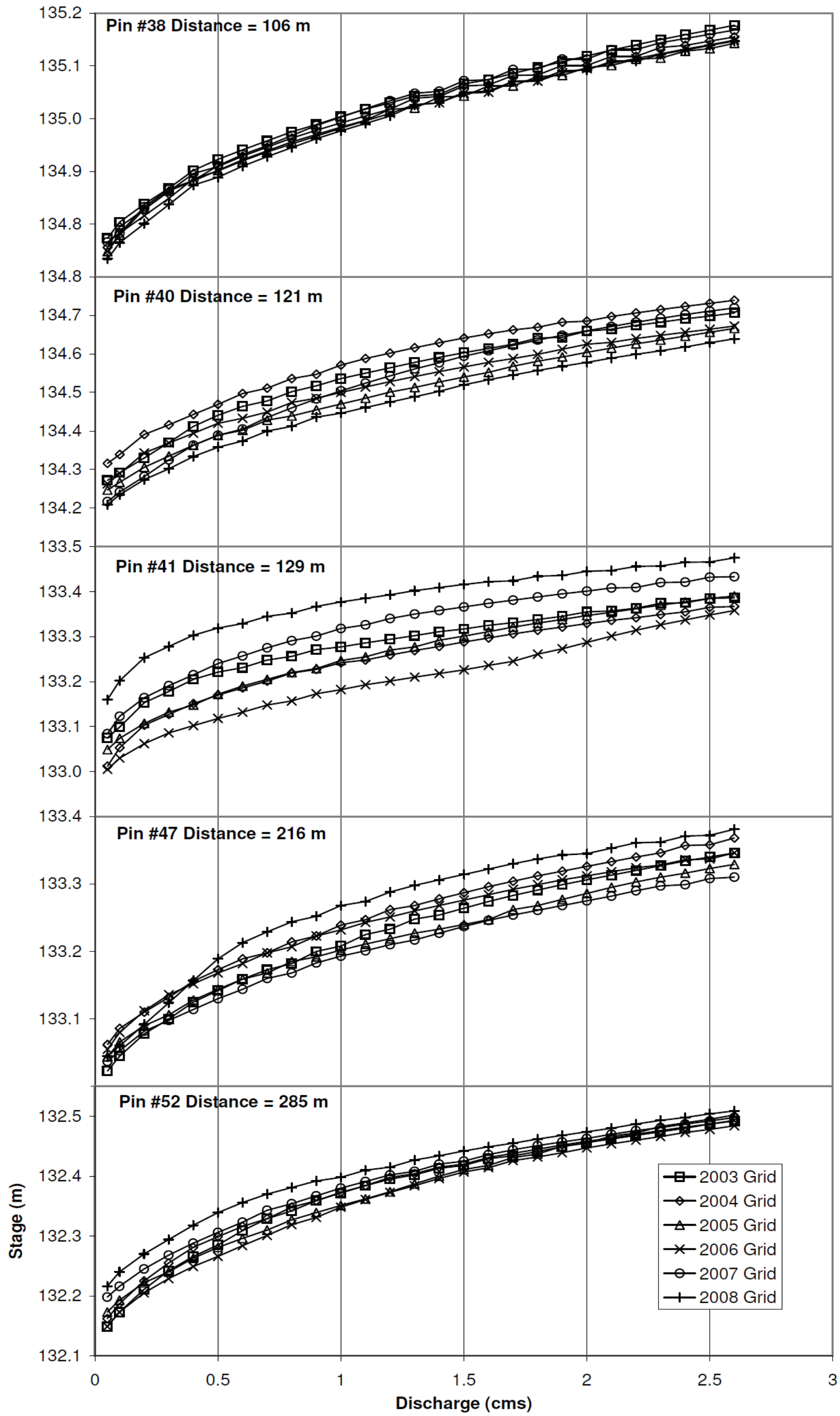

Figure 26: East Creek modeled stage-discharge at various pins for multiple years

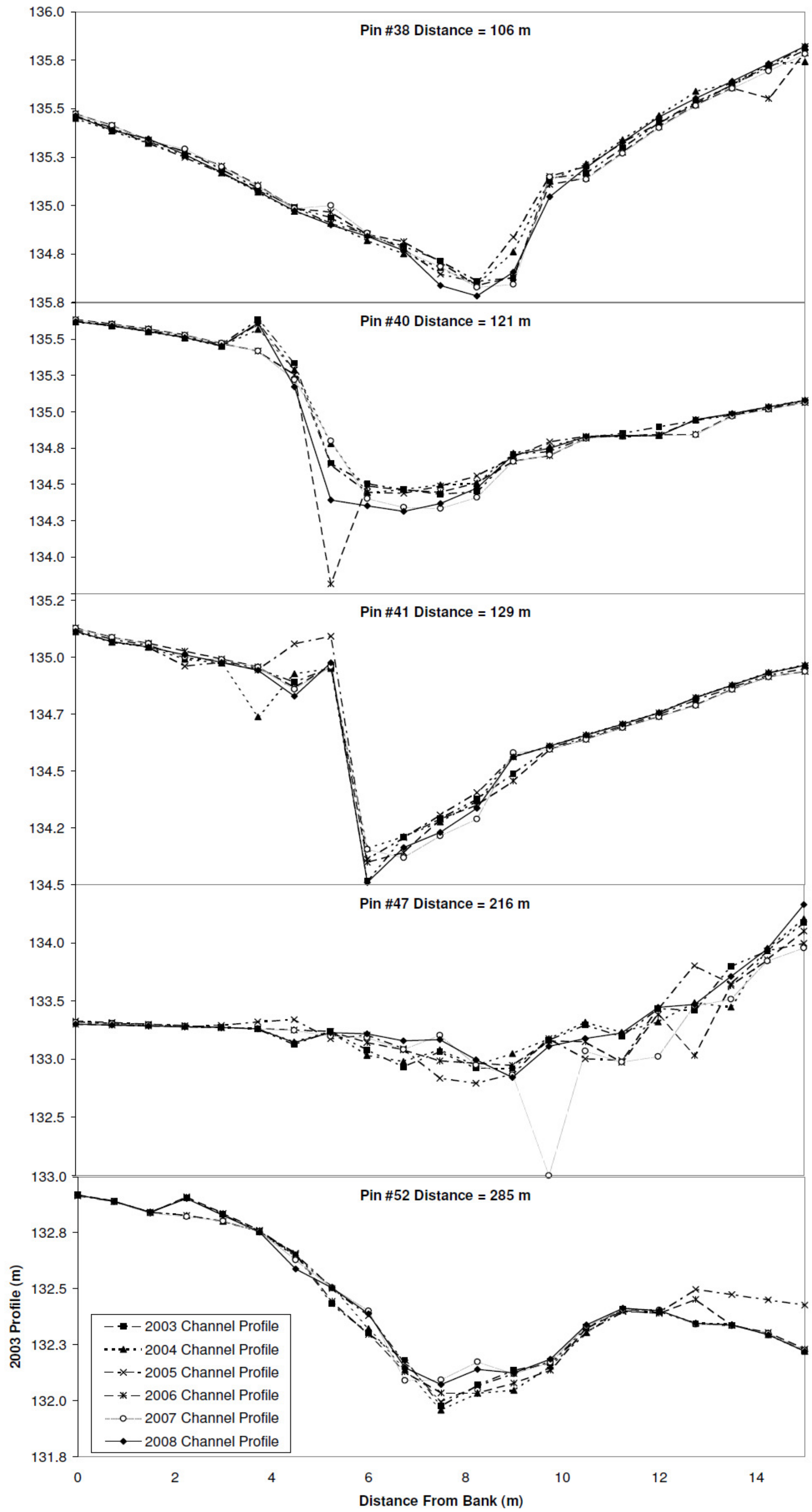

Figure 27: East Creek surveyed bed shape at various pins for multiple years

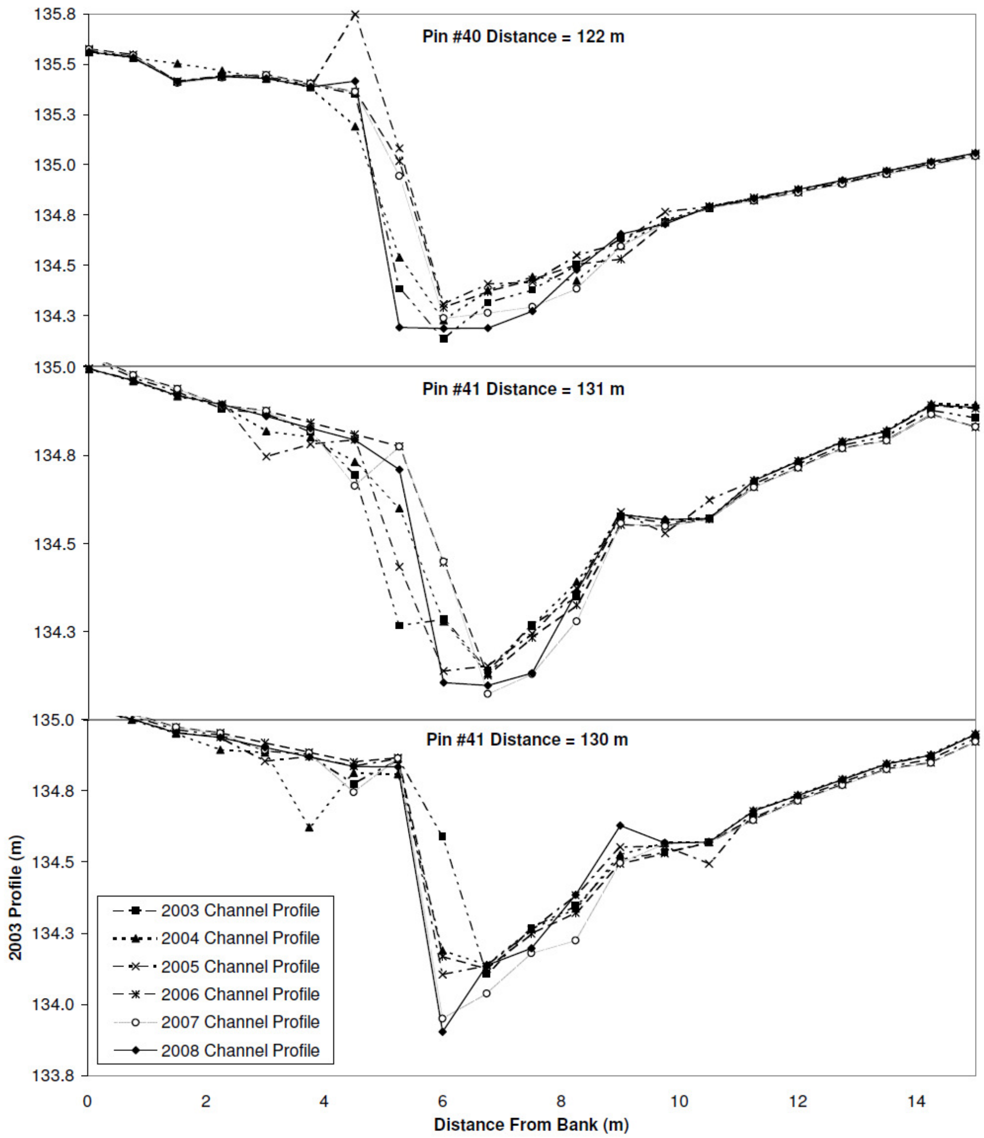

Figure 28: East Creek surveyed bed shape immediately downstream of the modelled locations for Pin #40 and #41

6 CONCLUSION

A one-dimensional model of momentum balance incorporated two roughness models to calculate theoretical stage-discharge relations at four sites in British Columbia that range in bed stability, bed structure, hydrology and sediment supply. To better account for the non-linear relationship between flow and the spatially-variable grain-size distribution, spatially-distributed roughness was incorporated into the Kean and Smith (2005) model. The standard topographic field survey was adjusted to include simple, specific measurements. This was combined with three new formulae for geometric parameters that reduce the overall uncertainty in the topographic input and eliminate assumptions from the roughness model.

The results show how (1) spatially-distributed roughness yielded better results than spatially-averaged roughness, (2) the stage-discharge relation shifted in response to a flood (Baker), and in response to annual bed movement (East Creek), and therefore, (3) the relations must be re-evaluated following events that mobilize the bed. For the two relatively stable reaches (Alouette and Cayoosh), (4) the modelled results were similar to those measured by the Water Survey of Canada and the method can be used to estimate high flows and flows in remote, stable locations.

Until new technology allows stream discharge to be measured directly, stage-discharge relations will remain a necessity. Accurate numerical modelling is crucial to define stage-discharge relations for new sites. For existing gauges the modelling can update the relations following any bed movement, which is particularly useful for the numerous unstable mountain-streams in BC. To ensure the numerical model is independent of the empirical approach of generating stage-discharge relations, the model cannot be calibrated to the same manual measurement used for the empirical approach. The empirical method is not practical for unstable beds, as the manual measurements are taken over a period of months or even years, in which time the beds shift. Numerical modelling provides an immediate stage-discharge relation from a single site survey. This is useful when hydrometric sites are created or moved, and as survey tools improve so do the speed and cost of surveys.

The model used in this study required no calibration, reducing the equifinality of parameters (Aronica et al., 1998, and Pappenberger et al., 2004) and provides an independent check on standard empirical methods. However, the level of validation was a coarse comparison between the model and measured stages for a given discharge. The validation could become more specific with more data, such as localized shear stress, sediment movement, and velocity profiles. This method can compliment the popular empirical approaches to developing stage-discharge relations, but to provide a realistic alternative to the popular approaches this model needs to be further validated for various bed types at high discharges.

7 REFERENCES

Aronica, G., B. Hankin, K. Beven (1998), Uncertainty and equifinality in calibrating distributed roughness coefficients in a flood propagation model with limited data, Advances in Water Resources, 22(4).

Baldassarre G. Di., A. Montanari (2009), Uncertainty in river discharge observations: a quantitative analysis, Hydrology and Earth System Sciences, 13, pp. 913–921.

Bhattacharya, B., D.P. Solomatine (2005), Neural networks and M5 model trees in modelling water level-discharge relationships, Neurocomputing, 63, pp. 381-396.

Bohorquez, P., and S.E. Darby (2008), The use of one- and two-dimensional hydraulic modeling to reconstruct a glacial outburst flood in a steep Alpine valley, Journal of Hydrology, 361(3).

Braca, G. (2008), Stage-discharge relationships in open channels: Practices and problems, FORALPS technical reports, 11. Università degli Studi di Trento, Dipartimento di Ingegneria Civile eAmbientale, Trento, Italy, 28, pp. 24.

British Columbia Conservation Foundation (1999), Alouette River Gravel Replacement, Prepared for BC Hydro Bridge Coastal Restoration Program, 99-LM-09.

British Columbia Conservation Foundation (2005), Habitat Assessments and Restoration Prescriptions for the Corrections Reach of the Alouette River, Prepared for BC Hydro Bridge Coastal Restoration Program, 05-AL-01.

British Columbia Conservation Foundation (2006), South Alouette River Fish Habitat Restoration Project, Prepared for BC Hydro Bridge Coastal Restoration Program, 06-ALU-03.

Cao, Z., P. A. Carling (2002), Mathematical modelling of alluvial rovers: reality and myth. Part 1: General review, Proceedings of the Institution of Civil Engineers, Water and Maritime Engineering, 154(3).

Carney, S. K., B.P. Bledsoe, and D. Gessler (2006), Representing the bed roughness of coarse-grained streams in computational fluid dynamics. Earth Surface Processes and Landforms, 31, pp. 736–749.

Caulkins, J.L., 2010. Sediment transport and channel morphology within a small, forested stream: East Creek, British Columbia. Unpublished dissertation, University of British Columbia, Vancouver.

Caulkins, J., M.A. Hassan (2007), Spatial and Temporal Patterns of Sediment Transport in a Small Stream, Eos Trans. AGU, 88(52), Fall Meet. Supplemental.

Chaudhry, M.H. (2008), Open Channel Flow, 2nd ed., pp. 151-197, Springer.

Chen, Y.C. and C.L. Chiu (2004), A fast method of flood discharge estimation, Hydrological Processes, 18, pp. 1671-1684.

Chow V. T. (1959), Open Channel Hydraulics, McGraw-Hill, New York.

Clancy, K. F., and K. L. Prestegaard (2006), Quantifying particle organization in boulder bed streams, in 4th Iahr Symposium on River, Coastal and Estuarine Morphodynamics, ed. G. Parker, and M.H. Garcia, Published by Taylor & Francis.

de Jong, C. (1995), Temporal and spatial interactions between river bed roughness, geometry, bedload transport and flow hydraulics in mountain streams—Examples from Squaw Creek (Montana, USA) and Lainbach/Schmiedlaine (upper Bavaria, Germany), Berlin. Geogr. Abh., 59, pp. 1–229.

DeGagne, M.P.J., G.G. Douglas, H.R. Hudson, S.P. Simonovic, (1996), A decision support system for the analysis and use of stage–discharge rating curves, Journal of Hydrology 184, pp. 225– 241.

Does, T., G. Morgenschweis, and T. Schlurmann (2002), Extrapolating stage-discharge relationships by numerical modeling, In: Proceedings 5th International Conference on Hydro-Science and Engineering (ICHE-2002), September 18–21, Warsaw, Poland.

Dottori, F., M. L. V. Martina, and E. Todini (2009), A dynamic rating curve approach to indirect discharge measurement, Hydrology and Earth System Sciences, 6, pp. 859–896.

Fischenich, C. and S. Dudley (2000). Determining drag coefficients and area for vegetation, EMRRP Technical Notes Collection, TN EMRRP-SR-8, U.S. Army Engineer Research and Development Center, Vicksburg, MS.

Folk, K. A., K. L. Prestegaard (2000), The Organization of Boulders and Associated Velocity Fields in Natural Streams, Eos Trans. AGU, 81 (48), Fall Meet. Suppl., Abstract NG71B-24.

Freeman, G.E., R.R. Copeland, and M.A. Cowan (1996), Uncertainty in Stage Discharge Relationships, in: Stochastic Hydraulics, Proceedings of the 7th Symposium on Stochastic Hydraulics, IAHR, pp. 601-608.

Freeman, G.E., W.H. Rahmeyer, and R.R. Copeland (2000), Determination of resistance due to shrubs and woody vegetation, Technical Report, ERDC/CHL TR-00-25, U.S. Army Engineer Research and Development Center, Vicksburg, MS.

Gawne D. K. and S. P. Simonovic, (1994), A computer-based system for modelling stage-discharge relationship in steady-state conditions. Journal of Hydrological Sciences, 39(5), pp. 487–506.

Green, J.C. (2005), Choice of Percentiles and Axes to Determine Grain Resistance, Journal of Hydraulic Engineering, 131(11).

Hamilton, S. (2009) Personal Communication.

Hardy, R.J. (2008), Geomorphology Fluid Flow Modelling: Can Fluvial Flow Only Be Modelled Using a Three-Dimensional Approach?, Geography Compass 2(1).

Hassan, M.A., M. Church, J. Rempel, and R.J. Enkin (2009), Promise, performance and current limitations of a magnetic Bedload Movement Detector, Earth Surface Processes and Landforms, 34, pp. 1022–1032.

Herschy, R. W. (2008), Streamflow measurement, 3rd ed., Taylor & Francis, New York.

Herschy, R.W. (1999) Uncertainties in Hydrometric Measuresurements. In: Hydrometry-Principals and Practices. 2nd ed, Chichester: Wiley, pp.355-371.

Horritt M.S. and P.D. Bates (2002), Evaluation of 1D and 2D numerical models for predicting river flood inundation, Journal of Hydrology 268 pp. 87–99.

Huthoff, F., D.C.M. Augustijn, and S.J.M.H. Hulscher (2006). Depth-averaged flow in presence of submerged cylindrical elements. In: Riverflow 2006, Proceedings of the Third International Conference on Fluvial Hydraulics, Lisbon, Portugal, Vol. 1, pp. 575-582.

Järvelä, J. (2002), Determination of flow resistance of vegetated channel banks and Floodplains, in River Flow , D. Bousmar and Y. Zech (editors), Lisse, Swets & Zeitlinger, pp. 311-318.

Jazizadeh, F., and A. Zarrati (2008), Development of a three-dimensional numerical model to solve shallow-water equations in compound channels, Canadian Journal of Civil Engineering. 35(9).

Juracek, Kyle E., F.A. Fitzpatrick (2009) ,Geomorphic applications of stream-gage information, River Research and Applications, 25(3), pp. 329-347.

Kean, J. W. (2003), Computation of flow and boundary shear stress near the banks of streams and rivers, Ph.D. thesis, 168 pp., University. of Colorado, Boulder.

Kean, J. W., and J. D. Smith (2005), Generation and verification of theoretical rating curves in the Whitewater River Basin, KS, Journal of Geophysical Research, 110, F04012, doi:10.1029/2004JF000250.

Lee, W.S., K.S. Lee, S.U. Kim, E.S. Chung (2009), The Development of Rating Curve Caonsidering Variance Function Using Pseudo-likelihood Estimation Method, Water Resouces Management, DOI 10.1007/s11269-009-9448-8

Leonard, J., M. Mietton, H. Najib, and P. Gourbesville (2000), Rating curve modelling with Manning's equation to manage instability and improve extrapolation, Journal of Hydrological Sciences, 45(5), 739–750.

Lisle, T. E., M. A. Madej (1992), Spatial Variation in Armouring in a Channel with High Sediment Supply, in Dynamics of Gravel Bed Rivers, P. Billi, R.D. Hey, C.R. Thorne and P. Tacconi (editors), John Wiley & Sons.

Lisle T. E., J. M. Nelson, J. Pitlick, M. A. Madej, B. L. Barkett (2000), Variability of bed mobility in natural, gravel-bed channels and adjustments to sediment load at local and reach scales, Water Resources Research, 36(12).

Lohani, A. K., N. K. Goel, and K.K.S. Bhatia (2006), Takagi-Sugeno fuzzy inference system for modelling stage-discharge relationship, Journal of Hydrology 331, pp. 146-160.

Marren, P. M., M. A. Hassan, Y. Alila (2009), Application of geomorphic threshold theory to a mountain pine beetle infested catchment, Baker Creek, British Columbia, Canada, unpublished manuscript.

Mandelbrot, B. (1967), How Long Is the Coast of Britain? Statistical Self-Similarity and Fractional Dimension, Science, 156, pp. 636–638.

McMillan, H., J. Freer, F. Pappenberger, T. Krueger, M. Clark (2009), Impacts of uncertain river flow data on rainfall-runoff model calibration and discharge predictions, Hydological Processes submitted manuscript.

Moyeed, R. A., and R. T. Clarke. (2005). The use of Bayesian methods for fitting rating curves, with case studies, Advances in Water Resources, 28, pp. 807-818.

Nikora, V. I., D. G. Goring, and B. J. F. Biggs (1998), On gravel-bed roughness characterization, Water Resources Research, 34(3).

Oldmeadow DF, M. Church (2006), A field experiment on streambed stabilization by gravel structures, Geomorphology, 78, pp. 335–350.

Pappenberger, F., K. J. Beven, M. Horritt, and S. Blazkova (2005), Uncertainty in the calibration of effective roughness parameters in HEC-RAS using inundation and downstream level observations, Journal of Hydrology, 302(1–4), pp. 46–69.

Pappenberger, F., P. Matgen, K.J. Beven, J.-B. Henry, L. Pfister, and P. de Fraipont (2006), Influence of uncertain boundary conditions and model structure on flood inundation predictions, Advances in Water Resources, 29, 1430–1449.

Parker, G. (1990), Surface-based bedload transport relation for gravel rivers, Journal of Hydraulilc Research, 28(4).

Petersen-Øverleir, A. (2006), Modelling stage-discharge relationships affected by hysteresis using the Jones formula and nonlinear regression, Journal of Hydrological Sciences, 51, pp. 365–388.

Rice, S. P., J. K. Haschenburger (2004), A Hybrid Method for Size Characterization of Coarse Subsurface Fluvial Sediments, Earth Surface Processes and Landforms, 29, pp. 373–389.

Schmidt, A.R., and B.C. Yen (2008), Theoretical Development of Stage-Discharge Ratings for Subcritical Open-Channel Flows, Hydraulic Engineering, 134(9).

Scordo, E.B., and R. D. Moore (2009), Transient storage process in a steep headwater stream. Hydrological Processes, 23, pp. 2671–2685.

Shrestha R. R., A Bárdossy, and F Nestmann (2007), Analysis and propagation of uncertainties due to the stage–discharge relationship: a fuzzy set approach, Journal of Hydrological Sciences 52(4).

Sivapragasam C., and N. Muttil, (2005), Discharge rating curve extension–A new approach, Water Resources Management, 19, pp.505-520.

Smart, G. M.(1999), Turbulent velocity profiles and boundary shear in gravel-bed rivers. Journal of Hydraulic Engineering, 125(2).

Smart, G. M. (2001). "A new roughness estimation technique for granular-bed flow resistance." Proc., XXIX IAHR Hydraulic Engineering Congress, Beijing.

Smart G.M., J. Aberle, M. Duncan, and J. Walsh (2004). Measurement and analysis of alluvial bed roughness, Journal of Hydraulic Research, 42, pp. 227-237.

Smart, G.M., M.J. Duncan, and J.M. Walsh (2002), Relatively Rough Flow Resistance Equations, Journal of Hydraulic Engineering, 128(6).

Souhar, O., and J.B. Faure (2009), Approach for uncertainty propagation and design in Saint Venant equations via automatic sensitive derivatives applied to Saar river, Canadian Journal of Civil Engineering, 36, pp. 1144-1154.

Stephan, U. and D. Gutknecht (2002), Hydraulic Resistance of Submerged Flexible Vegetation, Journal of Hydrology, 269(1–2), pp. 27–43.

Summit Environmental Consultants Ltd. (2002), Survey of Gravel Recruitment Needs: Middle Shuswap River, Bridge River, Seton River and Cayoosh Creek, Prepared for Fisheries and Oceans Canada, September 2002.

Traver, R. G. (1994), Modelling multiple critical depths, Journal of the American Water Resources Association, 30(1).

Whiting, P. J., W. E. Dietrich (1990), Boundary Shear Stress and Roughness over Mobile Alluvial Beds, Journal of Hydraulic Engineering, 116(12).

Wiberg P.L., and J.D. Smith (1991), Velocity distribution and bed roughness in high-gradient streams, Water Resources Research, 27(5).

Wilson, C., P.D. Bates, and J.M. Hervouet (2002), Comparison of turbulence models for stage-discharge rating curve prediction in reach-scale compound channel flows using two-dimensional finite element methods, Journal of Hydrology 257(1–4): pp. 42–58.

Wolman M G (1954), A method of sampling coarse river-bed material, Transactions of the American Geophysical Union, 35, pp. 951-956.

Wu, F.C., H.W. Shen, and Y.J. Chou (1999), Variation of roughness coefficients for unsubmerged and submerged vegetation, Journal of Hydraulic Engineering, 125(9), pp. 934- 942.

Yen, B.C. (1999), Discussion about "Identification problem of open-channel friction parameters", Journal of Hydraulic Engineering 125(5), pp. 552–553.

APPENDICES

APPENDIX A: DERIVATION OF GEOMETRIC FORMULAE

The St. Venant equations require the hydraulic radius or wetted perimeter, the flow depth and the cross-sectional area of flow. For gravel-bed rivers there is very little deviation between the surveyed perimeter and the actual wetted perimeter. For streams with large roughness the standard survey techniques typically have 1 m spacing and, therefore, do not provide enough resolution to accurately encapsulate the roughness elements. Fine resolution survey techniques such as laser profiling (Smart et al. 2004) continue to be refined but are not ready for general application.

Figure 15 illustrates how the surveyed perimeter can drastically underestimate the wetted perimeter and cross-sectional area of flow. For this study the survey technique was adjusted and since the roughness parameters were measured for calculating the friction, these parameters, based on the probablilistic average of the grain-size distribution of the bed material, were used to develop a method to adjust the wetted perimeter and area .

The survey method was conducted such that the survey points mark the local minimums between sediment (Figure 18). This was to help ensure the area of the large roughness elements could be independently superimposed on the area calculated from the survey points. At all the test sites, the grain sizes were measured and discrete log-normal distribution parameters calculated according to Wiberg and Smith (1991). This distribution was also mapped spatially to prevent non-weighted averaging of the distributions.

A.1 Cross-sectional Area of Flow

To complete the model an estimate of the cross-sectional area perpendicular to the flow needed to be calculated and subtracted from the surveyed cross section. Assuming a parabolic shape for the sediment (Smart et al 2004), and assuming half the sediment is located below the datum set by the survey, the cross-sectional area protruding into the flow and perpendicular to the approach velocity of a single pebble is $A_D = \frac{\pi}{4} D_y D_z$.

If we assume that $\frac{1}{2} D_y = D_z$ then the average cross-section area of all the sediment grains, averaged over all the grain-size classes [1,M], is

$$\overline{A_D} = \frac{\pi}{2}\left[\sum_{m=0}^{M} D_{z,m} c_m\right]^2 \tag{A.1}$$

The sediment diameter (D_m), sediment concentration (c_m), and topographic surveyed depth (h_{topo}) change across the cross section. Proportion of the surveyed wetted perimeter (P_{topo}) taken up by one average grain width (θ) is also the inverse of the number of average grains that fit in the topographic surveyed wetted perimeter.

$$\theta \approx \frac{\overline{D_y}}{P_{topo}} = \frac{2\overline{D_z}}{P_{topo}} = \frac{2}{P_{topo}} \sum_{m=0}^{M} D_{z,m} c_m \tag{A.2}$$

$$P_{topo} = \sqrt{(B)^2 + \left(h_{topo,0} - h_{topo,1}\right)^2} \tag{A.3}$$

The cross-sectional area of grains protruding into the flow and perpendicular to the approach velocity $\left(\overline{A}_{grains}\right)$ is

$$\overline{A}_{grains} = \frac{\overline{A}_D}{\theta} \tag{A.4}$$

This is similar to the blocking ratio described by Smart et al (2004); summing over all grain sizes

$$\overline{A}_{grains} = \frac{\pi P_{topo}\left[\sum_{m=0}^{M} D_{z,m} c_m\right]^2}{4\sum_{m=0}^{M} D_{z,m} c_m} \tag{A.5}$$

However the cross-sectional area of grains protruding above the water surface must be subtracted to accurately calculate the ‘wetted’ cross-sectional area facing the flow. This leads to:

$$\overline{A_D}\Big|_x = \frac{\pi}{2}\sum_{m=0}^{M} D_{z,m}{}^2 c_m{}^2 - \frac{\pi}{2}\sum_{m=whereD>h}^{M} \left(D_{z,m} - h_{topo}\right)^2 c_m{}^2 \tag{A.6}$$

$$\overline{A}_{grains\_submerged,i} = \frac{P_{topo,i}\pi}{4\sum_{m=0}^{M} D_{z,m,i}c_{m,i}}\left[\sum_{m=whereD_m\le h_i}^{M} D_{z,m,i}{}^2 c_{m,i}{}^2 - \sum_{m=whereD>h_i}^{M}\left(h_{topo,i}{}^2 - 2D_{z,m,i}h_{topo,i}\right)c_{m,i}{}^2\right] \tag{A.7}$$

$$A_{flow} = A_{topo} - \overline{A}_{grains\_submerged,i}$$

$$A_{flow} = \sum_{i=1}^{I}\left\{h_{topo}B_i - \frac{P_{topo,i}\pi}{4\sum_{m=0}^{M} D_{z,m,i}c_{m,i}}\left[\sum_{m=whereD_{m,i}\le h}^{M} D_{z,m,i}{}^2 c_{m,i}{}^2 - \sum_{m=whereD>h}^{M}\left(h_{topo,i}{}^2 - 2D_{z,m,i}h_{topo,i}\right)c_{m,i}{}^2\right]\right\} \tag{A.8}$$

Equation (A.7) is for a single segment (i) in the cross-section and hence (A.8) is the summation over all segments [1-I] in the cross-section.

The main errors/assumptions to this approach are: treating the shape of the sediment as a parabola, the assumed log-normal sediment distribution, and a lack of imbrication among the roughness elements.

A.2 Flow Depth

As a result of the survey method, the surveyed height for each cross-section is different from the flow depth (h_{flow}), which is back calculated using the wetted area (A_{flow}) defined above.

Since the cross-sectional area of flow is a function of the flow depth

$$A_{flow} = \int h_{flow}\,dy \tag{A.9}$$

the differential form of equation (A.8) can be used.

$$h_{flow} = \frac{dA_{flow}}{dy} = h_{topo} - \frac{dP_{topo}}{dy}dy\frac{\pi}{4\sum_{m=0}^{M} D_{z,m}c_m}\left[\sum_{m=whereD_m\le h}^{M} D_{z,m}{}^2 c_m{}^2 - \sum_{m=whereD>h}^{M}\left(h_{topo}{}^2 - 2D_{z,m}h_{topo}\right)c_m{}^2\right] \tag{A.10}$$

The surveyed perimeter and its derivative are calculated using the following equations

$$P_{topo,i} = \sqrt{(B)^2 + \left(h_{topo,0} - h_{topo,1}\right)^2} \tag{A.11}$$

$$\frac{dP_{topo}}{dy} = \frac{B}{\sqrt{(B)^2 + \left(h_s - h_{s,1}\right)^2}} + \frac{\left(h_{topo,0} - h_{topo,1}\right)\frac{dh_{topo}}{dy}}{\sqrt{(B)^2 + \left(h_{topo,0} - h_{topo,1}\right)^2}} \tag{A.12}$$

Unfortunately, equation dP_{topo}/dy is not defined at the endpoints. The best way to resolve this would be to solve the function as a limit approaching the endpoints but since the slope (dh_{topo}/dy) is very small we simply assumed

$$\frac{dP_{topo}}{dy} = 1 \tag{A.13}$$

and hence equation (A.14) is the flow depth for each subsection i.

$$h_{flow,i} = h_{topo,i} - \frac{\pi}{4\sum_{m=0}^{M} D_{z,m,i} c_{m,i}} \left[\sum_{m=whereD_m \le h}^{M} D_{z,m,i}{}^2 c_{m,i}{}^2 - \sum_{m=whereD>h}^{M} \left(h_{topo,i}{}^2 - 2D_{z,m,i} h_{topo,i}\right) c_{m,i}{}^2 \right] \tag{A.14}$$

A.3 Calculating the Wetted Perimeter

In the process of modeling the St. Venant equations a Hydraulic Radius needed to be provided. Yet in a shear stress equation this parameter is often not clearly defined (Smart 2001). Smart (2001) suggested using a 'volumetric hydraulic radius' where R_v = volume of overlying water per unit plan area of bed, which is effectively the wetted width divided by the cross-section volume. This provided convenience to power-law estimates of stage-discharge relationships as the channel width was used in place of wetted perimeter. However, the area of the bed would remain ambiguous.

Calculating the exact wetted perimeter (P_{flow}) is similar to calculating the length of the coast of Britain (Mandelbrot, 1967) as it depends upon the scale of measurement. In this case the size classes of the measured grain-size data limited the scale.

Again, the geometry of sediment grains is assumed to be represented as a symmetric parabola (Smart et al. 2004) as shown in Figure A.1.

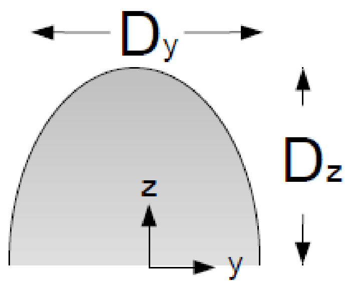

Figure A.1: Parabolic representation of a single sediment grain

The equation relating the x and z parameters along the circumference of the grain in Figure A.1 is

$$z = -\frac{4D_z}{D_y^{\,2}}x^2 + D_z \tag{A.15}$$

and the arc length from y = $-D_y/2$ to y = $D_y/2$ is calculated as

$$P_{grains}(x) = \int_{-D_y}^{D_y}\sqrt{1+4x^2\frac{D_z^{\,2}}{D_y^{\,4}}} = \frac{2D_z}{D_y^{\,2}}\int_{-D_y}^{D_y}\sqrt{\frac{D_y^{\,4}}{4D_z^{\,2}}+x^2}\,dx = \frac{x}{2}\sqrt{x^2+\frac{D_y^{\,4}}{4D_z^{\,2}}}+\frac{D_y^{\,4}}{8D_z^{\,2}}\ln\left(x+\sqrt{\frac{D_y^{\,4}}{4D_z^{\,2}}+x^2}\right)$$

If it is assumed that $2D_z=D_y$ (Wiberg and Smith 1991) then

$$dz/dx = -\frac{2x}{D_z}$$

$$P_{grains}(x) = \int_{-D_y/2}^{D_y/2}\sqrt{1+\frac{4x^2}{D_z^{\,2}}} = \frac{2}{D_z}\int_{-D_z}^{D_z}\sqrt{\frac{D_z^{\,2}}{4}+x^2}\,dx = \frac{2}{D_z}\left[\frac{x}{2}\sqrt{x^2+\frac{D_z^{\,2}}{4}}+\frac{D_z^{\,2}}{8}\ln\left(x+\sqrt{\frac{D_z^{\,2}}{4}+x^2}\right)\right]\Bigg|_{-D_z}^{D_z}$$

$$P_{grains}(x) = \left[\frac{x}{2}\sqrt{\frac{4}{D_z^{\,2}}x^2+1}+\frac{D_z}{4}\ln\left(x+\sqrt{\frac{D_z^{\,2}}{4}+x^2}\right)\right]\Bigg|_{-D_z}^{D_z}$$

$$P_{grains}(x) = \frac{2}{D_z}\left[\frac{D_z}{2}\sqrt{x^2+\frac{D_z^{\,2}}{4}}+\frac{D_z}{2}\sqrt{D_z^{\,2}+\frac{D_z^{\,2}}{4}}+\frac{D_z^{\,2}}{8}\ln\left(D_z+\sqrt{\frac{D_z^{\,2}}{4}+D_z^{\,2}}\right)-\frac{D_z^{\,2}}{8}\ln\left(-D_z+\sqrt{\frac{D_z^{\,2}}{4}+D_z^{\,2}}\right)\right]$$

$$P_{grains}(x) = 2D_z\left[\sqrt{\frac{5}{4}} + \frac{1}{8}\ln\left(\left(\sqrt{\frac{5}{4}}+1\right)/\left(\sqrt{\frac{5}{4}}-1\right)\right)\right] = 2.95789D_z$$

The average wetted perimeter of a grain is

$$\overline{P_{grains}} = 2.95789\sum_{m=0}^{M} D_{z,m}c_m \tag{A.16}$$

and the proportion of the wetted perimeter taken up by one average grain width (equation (A.2)) is

$$P_{flow,i} = \overline{P_{grains,i}}/\theta_i \tag{A.17}$$

Equation (A.17) is for a single subsection and it includes the perimeter of grains protruding above the water surface. The perimeter length above the water surface must be subtracted to get the wetted perimeter of flow (P_{flow}) for each subsection (i) then summed over the entire cross-section:

$$P_{flow} = \sum_i \frac{\sqrt{(B_i)^2 + \left(h_{topo,i} - h_{s,topo+1}\right)^2}}{2\sum_{m=0}^{M} D_{z,m,i}c_m} 2.95789\left[\sum_{m=0}^{M} D_{z,m,i}c_m - \sum_{m=whereD_z>h_i}^{M}\left(D_{z,m,i} - h_{topo,i}\right)c_m\right] \tag{A.18}$$

A.4 References

Mandelbrot, B. (1967), How Long Is the Coast of Britain? Statistical Self-Similarity and Fractional Dimension, Science, 156, pp. 636–638.

Smart, G. M. (2001). "A new roughness estimation technique for granular-bed flow resistance." Proc., XXIX IAHR Hydraulic Engineering Congress, Beijing.

Smart G.M., J. Aberle, M. Duncan, and J. Walsh (2004). Measurement and analysis of alluvial bed roughness, Journal of Hydraulic Research, 42, pp. 227-237.

Wiberg P.L., and J.D. Smith (1991), Velocity distribution and bed roughness in high-gradient streams, Water Resources Research, 27(5).

APPENDIX B: BED ROUGHNESS

B.1 Review

Roughness is primarily used to calculate the vertical-velocity profile (Lane, 2005) and is normally described as a Chezy (C), Manning (n) or Darcy Weibach (f) coefficient. The Darcy Weibach parameter is normally calculated using the Moody diagram (White, 1999), or empirically using simple power law or log law formulations (Keulegan, 1938; Gessler, 1990; Smart et al., 2002), or log laws that include sediment grain-size statistics (Leopold and Wolman, 1957; Hey, 1979; Parker and Peterson, 1980; Bathurst, 1982, 1985, 2002; Katul et al., 2002; Aberle and Smart, 2003; Cao et al., 2006; Ferguson, 2007; Comiti et al., 2007; Reid and Hickin, 2008, Zimmerman, 2009). A few studies have also tried to relate friction factors to the non-dimensional Froude and Reynolds numbers (Bathurst, 1982; Camacho and Yen, 1999; Cheng, 2007).

Manning's n is a popular empirical parameter that changes very little with stage and can be easily calibrated from simple slope-discharge-area measurements of a stream (Lang et al., 2004). It continues to be used in some commercial software (HEC-RAS, LISFLOOD-FP and TELEMAC-2D, Horritt & Bates, 2002). Many researchers have attempted to derive Manning's n using physically measurable parameters (see Lang et al. 2004 for a review of different empirical equations) and it has been derived based on the phenomenological theory of turbulence (Gioia and Bombardelli, 2002). The n coefficient is not physically-based, is site specific (Reid and Hickin, 2008), does not work well for large roughness elements, and must be assumed/estimated from field measurements (Chow, 1959; Hicks and Mason, 1991) with a large uncertainty (Freeman et al., 1996).

The dimensionless Chezy coefficient is typically related to the depth averaged velocity ($\bar{u}$) and the shear velocity (u^*):

$$C = \sqrt{\frac{8}{f}} = \frac{\bar{u}}{u^*} \qquad \textbf{(B. 1)}$$

One of the most popular velocity profiles is the log law (Nikuradse, 1933, Keulegan, 1938), which can be derived from a simple force balance and an eddy viscosity model (Kean and Smith, 2005). The log law relies on a roughness length (z_o) that can be calibrated from known stage-discharge measurements (Kean and Smith, 2005) or can be defined from the grain-size distribution (Wiberg and Smith, 1991, Yen, 1999, and Smart, 1999). Power law formulations are another option for the vertical velocity profile (Gessler, 1990, Barenblatt, 1993, and Dignman and Sharma, 1997) but these do not relate to the underlying physics.

For large scale roughness (Ferro, 1999, and Bathurst, 1982) the bed sediment occupies a significant proportion of the channel, blocking flow and causing funnelling. This can cause non-logarithmic velocity profiles (Byrd et al., 1999) and energy loss an order of magnitude greater than the skin resistance losses modeled by the log-law velocity profile (Bathurst, 1982). Several frictional relationships have been specifically developed for large scale roughness (Bathurst, 1978, Bathurst et al., 1981, Wiberg and Smith, 1991, Baiamonte et al., 1995, and Ferro, 1999 and references therein).

B.2 Wiberg and Smith (1991) Roughness Model

For large scale roughness, the algorithm developed by Wiberg and Smith (1991) was used to calculate the velocity profile $u` = (\bar{u}/u_*)$. This algorithm was also used by Kean (2003) and Carney et al (2006). The algorithm is physically based and accounts for the stochastic nature of the sediment distribution.

The algorithm separates the total shear (equation (B. 2)) into internal friction stress (τ_f) and drag stress on the roughness elements (τ_D).

$$\tau_T(z) = \tau_f(z) + \tau_D \qquad \textbf{(B. 2)}$$

Using a simple mixing length (L) eddy viscosity model to simulate the friction stress

$$\tau_f(z) = \rho u_{*f} L \frac{du}{dz} \qquad \textbf{(B. 3)}$$

and to ensure the local velocity scale is used Wiberg and Smith assume

$$u_{*f} = \left(\tau_f / \rho\right)^{1/2} \quad \textbf{(B. 4)}$$

The total shear can be calculated based on the boundary shear stress

$$\tau_T(z) = \rho u_T^{*2}\left(1 - \frac{z}{h}\right) = \rho g h S\left(1 - \frac{z}{h}\right) \quad \textbf{(B. 5)}$$

$$u_T^* = \sqrt{ghS} = \left.\sqrt{\frac{\tau_T(z)}{\rho}}\right|_{z=0\approx z_o} \quad \textbf{(B. 6)}$$

Combing the equations to this point to remove τ_T and τ_f and rearranging for the derivative

$$\frac{du}{dz} = \sqrt{\frac{ghS}{\rho}}\frac{1}{L}\left\{\left(1 - \frac{z}{h}\right) - \frac{\tau_D(z)}{\rho g h S}\right\}^{1/2} \quad \textbf{(B. 7)}$$

The drag stress on the roughness elements is defined

$$\tau_D(z) = \sum_{m=i(z)}^{M(z)}\left(\frac{F_D}{A_\tau}\right)_m - \tau_s \quad \textbf{(B. 8)}$$

where τ_s is included to ensure the surface area of particles sticking above the water surface are not included in the overall particle drag.

The drag force (F_D) and the protruding cross-sectional area of the bed roughness parallel (in the xy plane) to the approach velocity (A_τ) depend on the particle size category (m). Since pebble counts are sorted into discrete classes, the drag is represented as a sum from the smallest grains that exist at that elevation above the bed (i), to the largest grains (M).

$$F_D(m) = \frac{\rho}{2}\left(C_D u^2 A_{grains}\right)_m \quad \textbf{(B. 9)}$$

A_{grains} is the protruding cross-sectional area of the bed roughness perpendicular (in the yz plane) to the approach velocity. Assuming the entire particle is exposed to the flow, and not just the upper half, then

$$\tau_D(z) = \frac{3}{4}\rho\sum_{m=i}^{M}\left(C_D\left\langle u_{ref}{}^2\right\rangle c\right)_m \frac{D_{z,m}}{D_{x,m}} \quad \textbf{(B. 10)}$$

Assuming the particle concentration (c_m) can be modeled as a log-normal distribution

$$c(m)=\frac{c_b}{\sigma_\phi\sqrt{2\pi}}\exp\left[-\frac{1}{2}\left(\frac{\phi_m-\phi_{50}}{\sigma}\right)^2\right] \qquad \textbf{(B. 11)}$$

where c_b is the normalization factor to ensure the total concentrations add up to 1.0.

σ_ϕ is in ϕ units (ϕ=-$\log_2(D_x)$).

The reference velocity (u_{ref}), as defined by Kean & Smith (2006), is the velocity that would exist if the element where not there.

$$\left\langle {u_{ref}}^2 \right\rangle\Big|_m=\frac{1}{z-z_o}\int_{z_o}^{z_m}u^2dz\approx\frac{1}{D_{mz}}\int_{z_o}^{z_m}u^2dz \qquad \textbf{(B. 12)}$$

therefore

$$\tau_D(z)=\frac{3\rho}{4}\left[\sum_{m=i}^{M}\left(\frac{C_{d,m}c_m}{D_{x,m}}\int_{z_o}^{z}(u`)^2dz\right)+\sum_{m=i}^{M}\left(\frac{C_{d,m}c_m}{D_{x,m}}\int_{z}^{z_m}(u`)^2dz\right)\right] \qquad \textbf{(B. 13)}$$

$$\tau_S=\frac{3\rho}{4}\sum_{m=i}^{M}\left[\frac{C_{d,m}c_m}{D_{x,m}}\int_{z_o}^{z_s}(u`)^2\right] \qquad \textbf{(B. 14)}$$

where $(u`)=u`(z)=u(z)/u_T^*$

substituting τ_D into equation (B. 7)

$$\frac{\partial u`(z)}{\partial z}=\frac{1}{L}\left\{\begin{array}{l}\left(1-\frac{z}{h}\right)-\frac{3}{4}\left[\int_{z_o}^{z}(u`)^2dz\sum_{m=i}^{M}\frac{C_{d,m}c_m}{D_{x,m}}+\sum_{m=i}^{M}\left(\frac{C_{d,m}c_m}{D_{x,m}}\int_{z}^{z_m}(u`)^2dz\right)\right]\\ +\frac{3}{4}\sum_{m=i}^{M}\frac{C_{d,m}c_m}{D_{x,m}}\int_{z_o}^{z_s=h}(u`)^2dz\end{array}\right\}^{1/2} \qquad \textbf{(B. 15)}$$

Wiberg and Smith (1991) assumed $D_x=D_y=2.0D_z$, such that the vertical axis (D_z)of particles is the short axis.

For the length scale in eddy viscosity

$$L(z)=\begin{array}{ll}\left(1-\sum_{m=i}^{M}c_m\right)\frac{z\kappa(1-z/h)}{\sqrt{1-z/h}}+\kappa\sum_{m=i}^{M}c_mD_m & \{z/h\le 0.2\}\\ \left(1-\sum_{m=i}^{M}c_m\right)\frac{\kappa h/\beta}{\sqrt{1-z/h}}+\kappa\sum_{m=i}^{M}c_mD_m & \{z/h>0.2\}\end{array} \qquad \textbf{(B. 16)}$$

Equation (B. 16) is evaluated and integrated at each level ($z=z_m$) to get u` as a function of $z_m$. The resulting profile tends to have a small increase in u` below D_{max}, an inflextion point around the height of D_{max}, and a logarithmic profile above D_{max}.

The influence of the drag coefficient (C_d) was investigated and found to have negligible influence on the resulting Chezy and Boussinesq coefficients. C_d was set to 0.45 (a sphere) for the study. A formula for C_d of a sphere, based on the Reynolds number (Montes, 1997), was tested, as well as an eighth order sphere drag equation (Liao, 1998). The model was also tested by applying the drag coefficient for a cylinder (C_d=1.2) to all roughness elements that protrude above the water surface. The model was further tested setting C_d for each sediment class to a random number between 0.1, a smooth sphere, and 2.1, a brick (White, 1999). The indifference of the C_d values at different levels suggests the shape of the sediment does not influence the overall algorithm. An attempt was made to try and explain this indifference with limited success and the following is presented as a heuristic argument.

Equation (B. 15) can be roughly equated to an ordinary differential equation (ODE) that can be expanded into a 1st order Taylor series.

$$\frac{dy}{dx} = \left[\theta + C_d \phi y^3\right]^{1/2} \approx (C_d \alpha)(y^3 + \eta) + O(2) \qquad \textbf{(B. 17)}$$

The solution to which is

$$\frac{\sqrt{3}}{18}\left(2\log\left(\eta^{1/3} + y\right) - \log\left(\eta^{2/3} + y^2 - \eta^{1/3} y\right) - 2\sqrt{3}\tan^{-1}\left(\frac{1}{3}\left(\eta^{1/3} - 2y\right)\frac{\sqrt{3}}{\eta^{1/3}}\right)\right) = \alpha\eta^{2/3} C_d \left(z + \text{constant}\right)$$

The drag coefficient has only a scaling influence on the vertical axis, and both β and α are functions of z, L, c_m, D_m and h. Therefore, α and η appear to command the solution and C_d, in comparison, becomes insignificant when $C_d = 1.0 \pm 0.4$. However, this is not a proof and a more complete analytical analysis is needed.

B.3 References

Aberle, J., G. Smart (2003), The influence of roughness structure on flow resistance on steep slopes, Journal of Hydraulic Research, 41(3).

Baiamonte, G., V. Ferro, and G. Giordano (1995), Advances on velocity profile and flow resistance law in gravel bed rivers, Excerpta, Vol. 9, Cuen Press, Napoli, Italy, pp. 41–89.

Barenblatt G.I. (1993), Scaling laws for fully-developed turbulent shear flows. 1. Basic hypotheses and analysis. Journal of Fluid Mechanics, 248, pp.513–20.

Bathurst J. C. (1978) Flow resistance of large-scale roughness, Journal of the Hydraulics Division, ASCE, 104, HY12, pp. 1587-1603.

Bathurst J.C. (1985). Flow resistance estimation in mountain rivers. Journal of the Hydraulics Division, ASCE, 114, HY4, pp. 625-643.

Bathurst J.C., (1982), Flow resistance in boulder-bed streams, in *Gravel-bed rivers,* Hey, R.D., Bathurst, J. C., and Thorne, C. R., eds., Chichester, England, John Wiley and Sons, p. 443-465.

Bathurst, J. C. (2002), At-a-site variation and minimum flow resistance for mountain rivers, Journal of Hydrology, 269, pp.11– 26.

Bathurst, Li and D.B. Symons (1981), Resistance equation for large scale roughness, Journal of the Hydraulics division, ASCE, Dec 1981, HY 12, pp. 1593-1613.

Byrd T. C., D. J. Furbish, J. Warburton (2000), Estimating depth-averaged velocities in rough channels, Earth Surface Processes and Landforms 25, pp. 167-173.

Cao, Z., J. Meng, G. Pender, and S. Wallis (2006), Flow Resistance and Momentum Flux in Compound Open Channels, Journal of Hydraulic Engineering, 132(12).

Carney, S. K., B.P. Bledsoe, and D. Gessler (2006), Representing the bed roughness of coarse-grained streams in computational fluid dynamics. Earth Surface Processes and Landforms, 31, pp. 736–749.

Cheng, N. (2007), Power-law index for velocity profiles in open channel flows, Advances in Water Resources, 30, pp. 1775–1784.

Chow V. T. (1959), *Open Channel Hydraulics*, McGraw-Hill, New York.

Comiti F, L. Mao, A. Wilcox, E. Wohl, M.A. Lenzi (2007), Field-derived relationships for flow velocity and resistance in high-gradient streams, Journal of Hydrology, DOI: 10.1016/j.jhydrol.2007.03.021.

Dingman, S. L., and K.P. Sharma (1997), Statistical development and validation of discharge equations for natural channels, Journal of Hydrology, 199, pp. 13–35.

Ferguson, R. (2007), Flow resistance equations for gravel and boulder-bed streams, Water Resources Research, 43, DOI: 1029/2006WR005422.

Ferro V. (1999), Evaluating Friction factor for gravel bed channel with high boulder concentration, Journal of Hydraulic Engineering 125(7).

Freeman, G.E., R.R. Copeland, and M.A. Cowan (1996), Uncertainty in Stage Discharge Relationships, in: Stochastic Hydraulics, Proceedings of the 7th Symposium on Stochastic Hydraulics, IAHR, pp. 601-608.

Gessler, J. (1990), Friction factor of armored river beds, Journal of Hydraulic Engineering, 116(4), pp. 531–543.

Gioia, G., F. A. Bombardelli (2002), Scaling similarity in rough channel flows, Physical Review Letters, 88(1).

Hey, R. D. (1979), Flow resistance in gravel-bed rivers, Journal of Hydraulic Engineering, 105, pp. 365– 379.

Hicks, D. M., and P. D. Mason (1991), Roughness characteristics of New Zealand rivers, Water Resources Survey, DSIR Marine and Freshwater, Wellington.

Horritt M.S. and P.D. Bates (2002), Evaluation of 1D and 2D numerical models for predicting river flood inundation, Journal of Hydrology 268 pp. 87–99.

Katul, G., P. Wiberg, J. Albertson, G. Hornberger (2002), A mixing layer theory for flow resistance in shallow streams, Water Resources Research, 38(11).

Kean, J. W. (2003), Computation of flow and boundary shear stress near the banks of streams and rivers, Ph.D. thesis, 168 pp., University. of Colorado, Boulder.

Kean, J. W., and J. D. Smith (2005), Generation and verification of theoretical rating curves in the Whitewater River Basin, KS, Journal of Geophysical Research, 110, F04012, doi:10.1029/2004JF000250.

Kean, J. W., and J. D. Smith (2006), Form drag in rivers due to small-scale natural topographic features: 1. Regular sequences, Journal of Geophysical Research, 111, F04009, doi:10.1029/2006JF000467.

Keulegan GH. (1938). Laws of turbulent flow in open channels. Journal of Research of the National Bureau of Standards, 21, pp. 707–741.

Lane, S.N. (2005), Roughness – time for a re-evaluation?, Earth Surface Processes and Land 30, pp.251–253.

Lang, S., A. Ladson and B. Anderson (2004), A review of empirical equations for estimating stream roughness and their application to four streams in Vitoria, Australian Journal of Water Resources, 8(1), 69-82.

Leopold, L. B., and M. G. Wolman (1957), River channel patterns: Braided, meandering and straight, U. S. Geol. Survey Prof. Paper, 282-B.

Liao, S. (1998), The 8th-order drag coefficient formula of a sphere in a uniform stream: A simplified description, Communications in Nonlinear Science and Numerical Simulation, 3(4), pp. 256-260.

Montes, S. (1998), *Hydraulics of Open Channel Flow*, ASCE Press, Reston VA.

Nikuradse, J. (1933), Stroemumgsgesetze in raughen Roehren, Forshungs Geg. des Ingenieurwesens, Heft 361, translated from German as NACA Tech. Memo., 1292.

Parker, G., and A.W. Peterson (1980), Bar resistance of gravel-bed streams, Journal of Hydrology, 106, pp. 1559– 1573.

Reid, D. E., E. J. Hickin (2008), Flow resistance in steep mountain streams, Earth Surface Processes and Landforms, 33, pp. 2211–2240.

Smart, G. M.(1999a), Turbulent velocity profiles and boundary shear in gravel-bed rivers. Journal of Hydraulic Engineering, 125(2).

Smart, G.M., M.J. Duncan, and J.M. Walsh (2002), Relatively Rough Flow Resistance Equations, Journal of Hydraulic Engineering, 128(6).

White (1999), *Fluid Mechanics*, McGraw Hill.

Wiberg P.L., and J.D. Smith (1991), Velocity distribution and bed roughness in high-gradient streams, Water Resources Research, 27(5).

Yen, B.C. (1999), Discussion about "Identification problem of open-channel friction parameters", Journal of Hydraulic Engineering 125(5), pp. 552–553.

Zimmerman , A. (2009), Flow resistance in steep streams, revised manuscript submitted to Water Resources Research.